Is Aquatic Bioenergy with Carbon Capture and Storage a Sustainable Negative Emission Technology?:

Insights from a Spatially Explicit Environmental Life-Cycle Assessment

A Thesis Presented to

the faculty of the School of Engineering and Applied Science

University of Virginia

In Partial Fulfillment
of the Requirements for the Degree
Master of Science

Department of Engineering System and Environment

By

Angelica Jasmin Melara

May 2020

Highlights

- Spatially explicit LCA models offer insights on negative emission technologies
- The USA has a confluence of factors that make A-BECCS a possibility
- A-BECCS has some likelihood of being net-energy producing and net carbon-consuming
- Enhanced oil recovery allows for short term carbon sequestration via A-BECCS
- Algae bioenergy with CCS is possible, but supply chain reconfiguration is necessary

Abstract

It is anticipated that the achievement of the Paris Climate Agreement will require the widespread deployment of negative emission technologies (NETs). The most prominent NET is bioenergy with carbon capture and storage (BECCS), which is typically envisioned to use terrestrial crops as feedstock. A few recent studies have focused on aquatic BECCS (A-BECCS), which makes use of marine macroalgae feedstock, as a possible means of reducing water and land use. However, the high logistic complexity of the A-BECCS supply chain makes it likely that regional biophysical and socio-technical factors will strongly influence its overall favorability. Therefore, this study applies a life-cycle assessment (LCA) incorporating a geographic information system (GIS) framework to estimate the environmental impacts of A-BECCS over all stages of its life-cycle. Three candidate locations in the USA are evaluated based on seemingly good proximity to coastal regions and CO_2 storage; namely, East Coast, West Coast, and the Gulf of Mexico. Model outputs include energy return on investment (EROI), and net global warming potential (GWP). Additional metrics are explored to elucidate A-BECCS's carbon sequestration and energy use efficiency, which are biogenic carbon efficiency and net energy required to store a GT of carbon. Monte Carlo simulation is used to characterize distributions of model outputs. Results reveal that only the Gulf of Mexico configuration has any likelihood of achieving both net energy production (probability of EROI > 1= 29%) and net CO_2 sequestration (probability of GWP < 0= 6%), but the probability of achieving both together is very low (5%). The other locations exhibit net positive energy production (EROI > 1), but not net negative carbon sequestration (GWP > 0). These results call into question the feasibility of the modeled A-BECCS system as an energy-producing NET and offer insights into possible system reconfiguration. For example, anaerobic digestion offers very low EROI and creates multiple carbon-bearing waste streams, which strongly undercuts overall net CO_2 sequestration. Finally, it is observed that enhanced oil recovery (EOR) strongly contributes to net-energy production (EROI > 1) in the modeled A-BECCS system, but also strongly undercuts net CO_2 sequestration, which is arguably the main goal of any NET. To our knowledge, this is the first geographically explicit life cycle assessment of A-BECCS and a step toward understanding the logistic complexities with NETs.

Keywords: climate change, negative emission technology, algae biofuel, carbon capture and storage, life cycle assessment

1. Introduction

Negative emission technologies (NETs) are embedded within several integrated assessment models (IAMs), with the various models indicating that widespread deployment of bioenergy with carbon capture and storage (BECCS) will be critically important in achieving the 2°C target [1], [2]. This technology seeks to deliver simultaneous energy generation and net uptake of CO_2, via purposeful cultivation of biomass that is converted to a usable energy carrier and the resulting CO_2 is permanently sequestered in geological formations. To date, most BECCS research has focused on terrestrial bioenergy crops such as woody or herbaceous crops [3]; such that the corresponding systems may be referred to as terrestrial BECCS (T-BECCS) configurations. An excellent review of T-BECCS is detailed by Kemper et al. (2015), and a summary of research priorities is outlined by Stavrakas et al. (2018) [4], [5]. From this and other work, T-BECCS deployment at the level specified by various IAMs will dramatically increase the consumption of land, water, and other resources, which will likely intensify existing competition between food and energy crops [1], [2], [4]–[6].

An alternative BECCS approach that may help mitigate land use and freshwater consumption burdens involves offshore cultivation of marine bioenergy crops, most notably macroalgae (i.e., “seaweed” or “kelp”). This alternative is referred to as aquatic BECCS (A-BECCS). While A-BECCS is more appealing than T-BECCS when solely considering land and freshwater use, it is estimated that macroalgae natively occupy less than 2% of the ocean’s surface [7]. Therefore, intentional and intensive cultivation approaches must be deployed if A-BECCS is to be implemented at a large enough scale to facilitate meaningful climate change mitigation [7]–[9]. The logistics involved with large-scale macroalgae cultivation and energy generation from aquatic biomass requires complex supply chains and significant energy inputs, which could undermine the system’s nominal energy and carbon capture objectives. Only a few papers have quantitatively analyzed these possible tradeoffs to date.

A mass balance analysis by N’yeurt et al. (2012) evaluated the negative emissions potential of what the authors called “ocean afforestation” systems, in which nutrients are applied to enhance the growth of existing macroalgae communities [9]. The biomass is harvested into submerged geosynthetic containers, where it is then anaerobically digested. Differential dissolution at a depth of 200 m below the ocean surface facilitates low-energy separation of the biogas constituents. The methane (CH_4) fraction is transported onshore for conversion into bio-electricity, whereas the residual gases (principally CO_2) are compressed and transported to seafloor geosynthetic storage, an artificial geological storage strategy [8], [9]. The authors estimate that macroalgae forests covering 9% of the world’s ocean surface could produce 12 billion tons per year of methane, effectively replacing the world’s annual fossil fuel consumption, while concurrently capturing 53 billion tons per year of CO_2. The proposed ocean afforestation system therefore theoretically delivers the dual-energy and carbon goals of BECCS. The authors also articulate several appealing ecosystem services of the proposed strategy (e.g., food production, a reversal of ocean acidification, etc). However, the analysis does not quantify what energy inputs would be consumed by the system, nor does it compute an overall balance for global warming potential (GWP). It is therefore impossible to evaluate the energy and carbon sequestration efficiencies of the proposed platform.

Several related LCA studies have quantified the energy and climate impacts of systems in which macroalgae is cultivated offshore and then converted via anaerobic digestion into biomethane to supplant fossil fuels. Langlois et al. (2012) analyzed the digestion of untransformed whole seaweed or seaweed-derived alginate extraction residues to produce methane, which was then converted into bioelectricity, and/or various co-products (i.e., sodium alginate, compost, and liquid fertilizer) [10]. Seghetta et al. (2017) evaluated several scenarios in which ocean-grown seaweed is digested to produce biogas, which is combusted in a cogeneration engine to produce electricity and heat; digestate is also produced, which is applied to agricultural lands to improve crop yield and increase soil carbon [11]. Both sets of authors reported reduced climate change impacts compared to a relevant fossil fuel benchmark. However, the systems modeled in both studies were not intended to deliver net negative CO_2 emissions, such that they cannot be construed as A-BECCS configurations. Hughes et al. (2012) also analyzed carbon flows through a system in which macroalgae is cultivated offshore and then converted via anaerobic digestion into biomethane and digestate [12]. However, the authors placed special emphasis on tracking dissolved organic carbon (DOC) that is fixed and released by the macroalgae during the cultivation phase, apportioning it into two pools: labile DOC (lDOC), which is quickly mineralized to CO_2 and re-released to the atmosphere; or refractory DOC (rDOC), which persists indefinitely in the ocean. The authors posit that because the rDOC is effectively permanently sequestered, rDOC production via managed macroalgae cultivation could constitute a negative emissions technology. They refer to this approach as an example of "bioenergy with biological carbon capture and storage" (BEBECCS). The authors estimate the CO_2 uptake of this approach is approximately 80 tC/km2/year. To contextualize this quantity, they indicate that achieving 10% of a well-known sequestration goal (320 GtC in 100 years) would require macroalgae farming on 17% of the global territorial sea area. Notably, this analysis is largely conceptual. It does not quantify energy inputs or outputs, nor does it compute what GWP impacts will arise during the operation of all the required subprocesses (e.g., cultivation, transport, digestion, etc). Thus, it is not possible to compute the energy and carbon sequestration efficiencies of the proposed approach.

From these studies and other, less quantitative reports, several possible supply chain configurations could be utilized for A-BECCS. Figure 1 illustrates the various options for each stage of the A-BECCS life-cycle and highlights the configuration that was evaluated in this study [4], [5], [13]. A hybrid configuration has also been proposed that includes both terrestrial and aquatic biomass, but was excluded from this analysis [14].

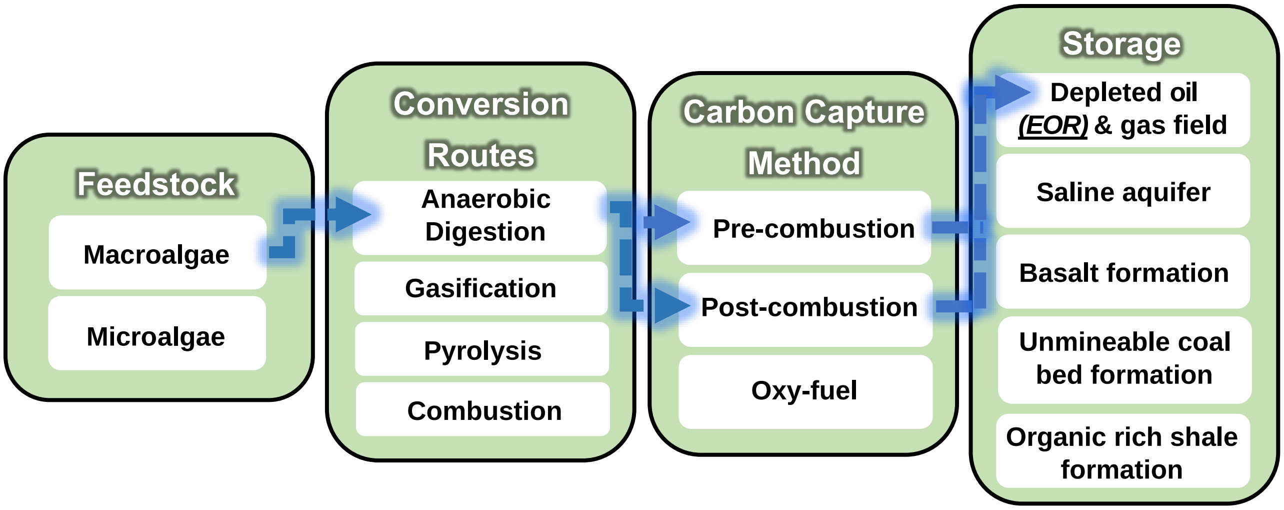

Figure 1. Visual summary of A-BECCS components by life-cycle stage. Dashed blue arrows illustrate the sequence of processes selected for analysis in this study.

The goal of this study was to evaluate whether an A-BECCS system making use of currently achievable technologies has promising potential as an energy-producing NET. A cradle-to-grave LCA model incorporating a geographic information system (GIS) framework was constructed to compute key energy and climate change performance metrics for three hypothetical systems in seemingly appealing locations within the conterminous USA; i.e., East Coast, West Coast, and the Gulf of Mexico. The key motivating hypothesis of this work was that different locations will exhibit different suitability for A-BECCS deployment based on the confluence of factors that are critical to achieving the dual-energy and net CO_2 sequestration goals of BECCS. These factors include high productivity, dense urban population centers with high power demands, good proximity to high-quality enhanced oil recovery (EOR) installations, and favorable marine transport networks. To our knowledge, this study is the first of its kind to make use of detailed geospatial information to assist in the evaluation of large-scale A-BECCS deployment in the USA.

2. Methods

This section summarizes the high-level modeling framework used for this study. The Appendix provides additional detailed information.

2.1. Overview, Systems Boundaries, and Functional Unit (FU)

The modeled A-BECCS system comprised six life-cycle stages: 1) aquaculture; 2) wet biomass transport; 3) pretreatment and digestion of the biomass with subsequent bio-methane concentration (upgrading) and transport, along with management of solid and liquid digestate residuals; 4) bio-electricity generation with CO_2 capture and compression; 5) CO_2 transport via pipeline, and 6) use of CO_2 for enhanced oil recovery (EOR). These stages and the system's boundaries are illustrated in Figure 2. The LCA-GIS modeling framework accounted for carbon flows throughout all stages, making appropriate provisions for transformation into various solid, liquid, and gaseous forms. LCA calculations were performed using Microsoft Excel with the Crystal Ball plug-in to automate Monte Carlo simulations (n = 50,000 trials per simulation). ArcGIS Pro 2.3.0 (ESRI, 2018) was used for mapping system components.

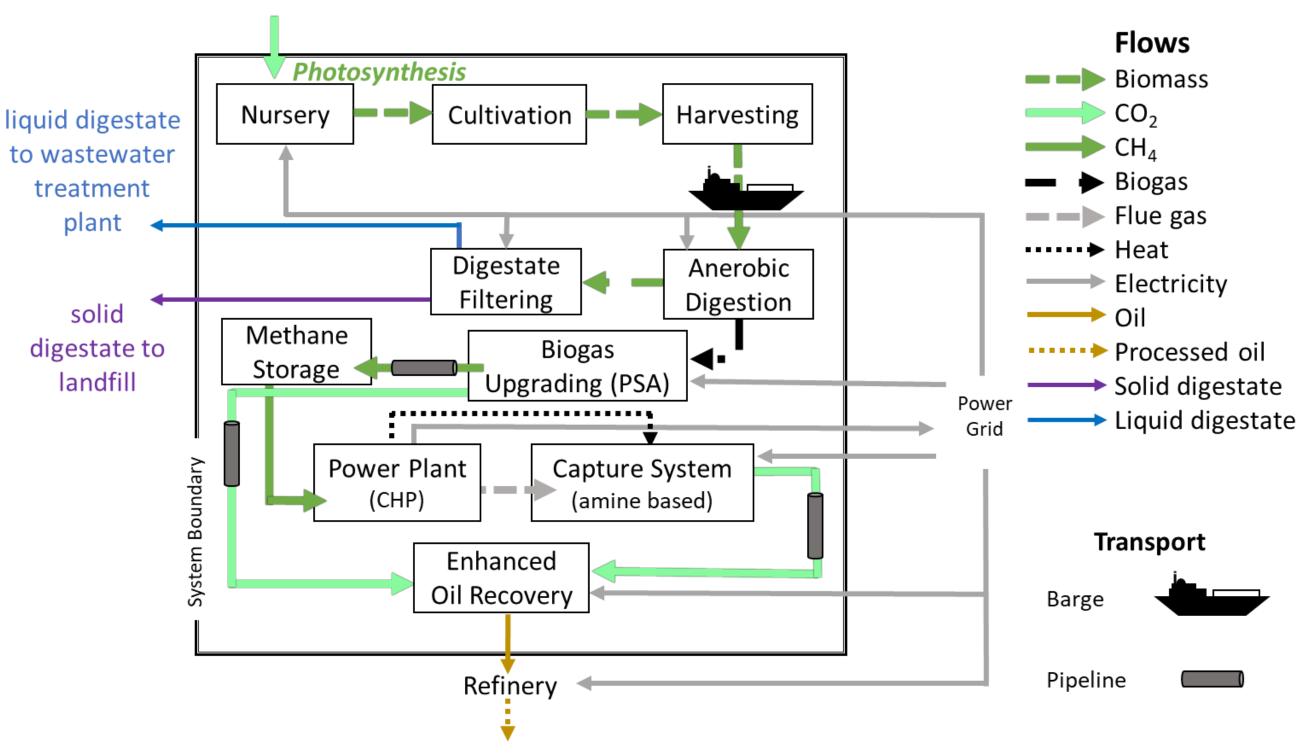

Figure 2. Process flow diagram for the modeled A-BECCS system. The web version of this article provides color versions of this and other figures.

The three candidate locations for A-BECCS deployment were selected based on their adjacency to coastal regions with well-demonstrated productivity (i.e., macroalgae yield) and geological formations with good suitability for enhanced oil recovery (EOR) [15]–[17]. It was assumed that harvesting, cultivation, and biomass transport occur offshore near the selected port of entry, while all other processes are performed on land. Specific regional land footprints were delineated by a 300-mi radius around suitable EOR storage locations within each general region. This distance is consistent with previous CO_2 source-sink analyses incorporating a GIS framework [18]. Ports were chosen based on ranked annual cargo capacity, proximity to geological storage, and a preference for longer barge transport distances (to collect biomass) was given so shorter pipeline distances to transport CO_2 were possible [17].

The functional unit (FU) was defined as annual power demand within the region bounded by the 300-mi radius around three potential geological storage sites (EOR), based on measured power plant location and capacity information collected from open source EIA data [19]. It was assumed that existing power plant facilities will be made compatible with A-BECSS in the future (i.e., by co-combusting macroalgae and coal, then capturing resulting CO_2). It was also assumed that existing natural gas transportation infrastructure will be used such that new pipeline construction will not be needed. Infrastructure impacts associated with the construction of anaerobic digestion facilities and power plants were similarly excluded. Digestion facilities are assumed to be located adjacent to ports resulting in negligible environmental burdens from truck biomass transport from port to digestion facility. In contrast, it was assumed that new CO_2 transportation infrastructure will be required, and the construction burdens were accounted for as part of this analysis. For comparison among systems, model outputs from the three regional clusters were scaled to a common basis of per-1 kWh.

The East Coast (EC) system assumes that Savannah, Georgia is the principal port of entry for marine biomass with aquaculture occurring along the coast of various eastern states (from Maine to Florida). Geologic storage is located in Alabama, Mississippi, and Louisiana. The Gulf of Mexico (GM) region assumes that Houston, Texas is the principal port of entry for marine biomass. Aquaculture occurs principally in Texas and Florida, and geologic storage is located in the Permian Basin (i.e., western Texas and New Mexico). The West Coast (WC) system assumes that Los Angeles, California is the principal port of entry for marine biomass. Aquaculture occurs along the coasts of California and Oregon, and geologic storage is primarily located in Southern California. Table 1 summarizes relevant information for each modeled region, including annual power demand (GWh), average emission factors (gCO2eq/kWh) for each local electricity grid, and annual average air temperature at each port [19]–[21].

Table 1. Annual power generation, average temperature at port, and state emission factors for the three modeled locations.

Geographic Region	Annual Power Generation (GWh) [19]	Average port temperature (°C) [21]	Average regional grid emissions (gCO_2/kWh) [20][1]
East Coast (EC)	590,885	19.33	511
Gulf of Mexico (GM)	127,039	20.58	577
West Coast (WC)	218,571	17.66	232

[1] *"EC" emissions factors correspond to Alabama, "GM" emissions factors correspond to Texas, and "WC" emissions factors correspond to California.*

2.2. Macroalgae Aquaculture (i.e. Nursery, Cultivation, and Harvest)

It is anticipated that purposeful, intensive macroalgae cultivation, as opposed to the collection of naturally grown biomass, will be required to support widespread A-BECCS deployment. Therefore, the biomass cultivation stage of the A-BECSS life-cycle was modeled based on parameters adapted from marine aquaculture literature. First, spore propagation and preparation occur in an onshore nursery [22]. Once they are sufficiently well established, the plantlets are transported to the open ocean via barge and cultivated offshore on 100-m lines (ropes) (Figure A1) [23]. Data limitations made it challenging to accurately quantify the growth and digestibility of individual macroalgae species by region; therefore, it was assumed that all three geographic locations produce the same hypothetical mixture of brown macroalgae that principally includes *Saccharina latissima, Laminaria digitata, Sargassum muticum*, and *Macrocystis pyrifera*. Existing literature documents the growth of these strains in all three modeled locations and under widely varying environmental conditions [16], [24]–[27]. The fresh weight yield used to calculate the ocean footprint area for regional clusters is static at 2 kg/m^2, a conservative value [28]. Table 2 summarizes relevant biochemical parameters for the assumed macroalgae biomass, including the ratio of volatile solids to total solids, carbon content, nitrogen content, phosphorus content, and water content on a fresh weight [FW] basis.

Macroalgae is then mechanically harvested via barge and transported to the regional port. Energy use and global warming potential (GWP) impact factors for aquaculture which incorporates the nursery (i.e., hatchery), open ocean cultivation, and harvesting phases were assigned a triangular distribution with likeliest= 0.59 kWh/kgTS, minimum=0.54 kWh/kgTS, maximum=0.65 kWh/kgTS, and likeliest= 0.11 $kgCO_2/kgTS$, minimum=0.10 $kgCO_2/kgTS$, maximum= 0.12 $kgCO_2/kgTS$, respectively [23]. Barge travel distance varied with ocean footprint areas required to deliver the FU for each regional cluster. For all regions, barge travel distance corresponded to the centroid distance of the required cultivation area. We assumed the biofuel supply to originate from the centroid of ocean growing areas, as calculated by the “Find Centroids” tool in ArcMap 10.6. Accordingly, the barge transport distance was calculated as the point distance between these centroids and corresponding ports of those clusters. Transportation impact factors for barge were 0.64 MJ_{eq}/t-km and 0.05 kg CO_2/t-km, from Ecoinvent (transport, freight, inland waterways, barge, RER with a carrying capacity of 15,000 tonnes) [29].

Finally, CO_2 uptake into refractory DOC (“blue carbon”) during macroalgae cultivation was not accounted for in this analysis, in light of the documented uncertainty and unresolved technical questions referenced in relevant literature [30], [31].

2.3. Biomass Pretreatment, Digestion, and Biogas Upgrading

Macroalgae pretreatment corresponds to mechanical cutting and homogenization of the raw biomass. Macroalgae pretreatment does not include drying. This processing consumes 38 kWh per ton of dry weight (DW) [23], [32]–[34]. This pretreatment significantly enhances digestibility and methane yield by increasing surface area and thereby making the substrate more bioavailable to anaerobic microorganisms [35]–[38].

The anaerobic digester is modeled as a continuously stirred tank reactor operated under mesophilic conditions (35^0C). Elemental composition and other digestion-relevant feedstock parameters of the hypothetical macroalgae feedstock are presented in Table 2. Lack of data made it impossible to parameterize feedstock biochemical differences for the three growing regions.

Table 2. Biochemical parameters of biomass

Input	Unit	Min	Likely (Median)	Max	Distribution	Source
Ratio of Volatile Solids (VS) to Total Solids (TS)	gVS/TS	548	656	763	Triangular	[39]–[46]
Carbon Content	%TS	23.70	33.00	39.14	Triangular	[39], [41]–[44], [47]
Nitrogen Content (N)	%TS	0.97	2.43	3.88	Triangular	[35], [39], [40], [48]
Phosphorus Content (P)	%TS	0.20	0.36	0.51	Triangular	[35], [39], [40]
Water Content	% Fresh Weight (FW)	75.00	81.50	85.00	Triangular	[46], [49], [50]

To compute the mass of macroalgae required to deliver 1 FU, total power plant output (Section 2.4) was divided by methane’s higher heating value (HHV) (55 MJ/kgCH_4) and methane’s density (0.66 kg/m^3 at 20 °C, 1 atm) [51]–[53]. The resulting mass of methane was then divided by biomethane potential (BMP) in kgCH_4/gVS (Table 3) and corresponds to the assumed anaerobic digestion conditions. Table A2 presents detailed information about relevant BMP values collected from the literature. The resulting macroalgae mass was then multiplied by the VS/TS ratio (i.e., ash-free dry weight [AFDW] fraction) (Table 2) to account for the presence of inert, non-digestible material in the raw feedstock because only VS can be converted into methane. Table 3 summarizes the digestion modeling parameters. It was assumed that digestion biogas comprises primarily methane (CH_4) and CO_2.

Table 3. Anaerobic digestion parameters

Input	Unit	Min	Likely (Median)	Max	Distribution	Source
Biomethane Potential (BMP)	Nm^3/g VS	1.54E-04	2.32E-04	3.11E-04	Triangular	[35], [42], [43], [54]–[62]
Methane percentage of biogas	% of biogas	42.26	47.30	57.48	Triangular	[32], [46], [56]
VS biodegradability	% VS added	53.49	58.23	62.98	Triangular	[42], [45], [60]
Loading rate (continuous reactors)	gVS/L-day	0.08	1.90	3.5	Triangular	[42], [43], [57]
Retention time	Days	12	30	40	Triangular	[35], [42], [43], [54]–[57]
Mesophilic temperature	^{0}C	30	35	40	Triangular	[35], [42], [43], [54]–[57]
Fugitive emissions from digester (L_{AD})	%	0.00	0.05	0.10	Triangular	[63], [64]

Energy consumption during anaerobic digestion was estimated based on an empirical regression equation from Soda et al. (2010) [65]. The original formulation was calibrated over a range of sludge loading weights up to a maximum of 40 tonnes TS per day. Because this value is less than the total mass of feedstock required to deliver 1 FU, it was assumed that multiple digesters are used in parallel. Per Soda et al., digester electricity consumption at the maximum sludge loading rate is 67.1 kWh per tonne TS. This quantity is multiplied by the total mass of feedstock required per FU, and it is assumed that electricity comes from the local grid (Table 1).

Heat consumption during anaerobic digestion (q_{AD}) was estimated by calculating heat required to maintain water input at a constant temperature of 35°C inside the digester at each of the modeled locations, with differences in average annual air temperature at each modeled location being considered (Table 1). This quantity was computed using Equation 1. Where m is the digester's flow rate, based on the mass of macroalgae required to deliver 1 FU. It was assumed that the digester feed has an initial water content of approximately 85% with essentially the same specific heat value as water (C_P = is 4,200 joules/kg°C). Digester heat loss was assigned a triangular distribution based on empirical data for municipal wastewater treatment plant digesters: minimum = 14%, maximum = 17%, and likeliest value = 15% [66]. Heat is supplied by an on-site boiler burning natural gas, HHV = 53 MJ/ kg, and efficiency = 86% [67]. Corresponding energy and GWP impact factors for natural gas were 1,116 KJ/MJ natural gas and 7.5E-03 $kgCO_{2eq}$/MJ [29], [68].

$$q_{AD}\left\{\frac{kJ}{kWh}\right\} = m\left\{\frac{kgH_2O}{kWh}\right\} \times c_P\left\{\frac{J}{kg^oC}\right\} \times \Delta T \times \left(1+\frac{q_{AD-loss}}{100}\right) \times \frac{1kJ}{1{,}000J} \qquad Eq.1$$

Belt filter pressing (BFP) is used to dewater the post-digestion slurry, which comprises a mixture of liquid and solids (i.e. digestate). Digestate is on average 11% solids, which are captured into a solid cake after dewatering [69]. Likeliest electricity consumption for BFP is 134.2 kWh/tTS and was assigned a triangular distribution, minimum= 122.02 kWh/tTS, and maximum= 147.65 kWh/tTS [65]. The dewatered solids are sent to a well-managed municipal landfill. Liquid waste is sent to a municipal wastewater treatment plant. Energy and materials consumption for solid and liquid residuals management were excluded from this analysis. However, their corresponding GWP emissions were included (Section 2.6).

Digestion biogas is upgraded (i.e. separated and concentrated) via pressure swing adsorption (PSA), which separates the CH_4 from the CO_2 and various trace gases. A PSA schematic is available in the SI showing gas flows. Electricity consumption for PSA was assigned a triangular distribution with minimum = 0.23 kWh/Nm^3, maximum = 0.28 kWh/Nm^3, and likeliest value = 0.25 kWh/Nm^3, as supplied by the local grid [70]. The CH_4 fraction is transmitted via existing pipeline infrastructure to a combined heat and power (CHP) plant. The CO_2 fraction is transported via small feeder pipelines to larger transmission pipelines, where it is commingled with post-combustion CO_2 from power plants. From there it is transported to a long-term geological storage location to conduct enhanced oil recovery. Section 3 of the Appendix presents additional detailed modeling information for anaerobic digestion, including pretreatment, upgrading biogas, belt filter pressing, and alternative biomass storage considered but not included in this analysis.

2.4. Power Plant Operations: Bio-Electricity Generation and CO_2 Capture

Bio-CH_4 from anaerobic digestion is stored onsite at a CHP plant as is standard practice for coal power plants in the US to maintain at least 60-90-day supply of fuel on-site [71]. Likeliest fugitive emissions losses during storage account for 0.36% of total bio-CH_4 mass and assigned a triangular distribution (minimum= 0.20%, maximum= 0.50%) while energy needed to compress gas is also assigned a triangular distribution with likeliest= 0.21 MJ/m$^3CH_4$, minimum= 0.91MJ/m$^3CH_4$ and maximum= 0.23 MJ/m$^3CH_4$ [72].

It was assumed that the CHP facility operating without carbon capture delivers electrical efficiency of 33% and thermal efficiency of 43% [73], but that the overall efficiency is reduced when a carbon capture technology is implemented. Therefore, the mass of methane required to deliver the FU as net electricity export was computed using Equation 2. This formulation accounts for the energy penalty (Energy Penalty$_{CCS}$) associated with the carbon capture rate (likeliest 90%), as well as methane losses during digestion (L_{AD}), PSA (L_{PSA}), transport (L_T), and storage (L_S), and uses an HHV for methane = 55 MJ/kg. Accordingly, the total amount of energy that must be produced by the power plant to deliver the FU is larger than the nominal FU itself. Other key power plant parameters are summarized in Table 4. Distributions for fugitive emissions are given in Table 4.

$$CH_4 \left\{\frac{kg}{kWh}\right\} = \frac{1\ kwh + Energy\ Penalty_{CCS}\{kWh\}}{\eta_{\mathrm{elec}}\{\%\}\ \times HHV\ \times \frac{0.277\ kWh}{MJ}} \times (1 + L_{AD}) \times (1 + L_{PSA}) \times (1 + L_T) \times (1 + L_S) \quad Eq. 2$$

The assumed CO_2 capture technology in the CHP plant for this study was monoethanolamine (MEA), an absorption process by an amine-based chemical solvent [13]. As evident from Equation 2, this technology reduces the electrical efficiency of the CHP facility. CHP heat is also consumed by the MEA process to regenerate solvent, and adequate recovered heat is available from the power plant, and therefore additional heat is not required [74]. More information and equations concerning power generation and heat reuse are in section 4.2 of the Appendix.

Table 4. Power plant and fugitive emission modeling parameters

Input	Units	Min	Likely (Median)	Max	Distribution	Source
Electrical efficiency (η_{elec})	%	-	33	-	-	[73]
Thermal efficiency (η_{TE})	%	-	43	-	-	[73]
CO_2 capture rate (CR)	%	75	90	90	Triangular	[74]
Load capacity factor	%	70	80	90	Triangular	[75]
Power plant size	MW	-	953	-	-	[19]
Loss of methane from PSA (L_{PSA})	%	2.3	2.5	2.8	Triangular	[76], [77]
Fugitive emissions from methane transport (L_T)	%	0.10	0.16	0.22	Triangular	[78], [79]
Fugitive emissions from methane storage (L_S)	%	0.20	0.36	0.50	Triangular	[80]
Energy consumption for carbon compression (Energy$_{CC}$)	kWh/ kgCO_2	-	0.15	-	-	[74]

2.5. CO_2 Transport and Storage

CO_2 sources were assigned to existing fossil fuel power locations [19], [81]. It was presumed that these locations can be made A-BECCS compatible in the future. CO_2 sinks were assigned to locations with appropriate reservoirs for EOR which have: appropriate porosity, thickness, permeability (for injectivity), a sealing caprock or confining unit, and a stable geological environment [18], [82]–[85][17]. As noted in Section 2.1, all CO_2 sources mapped to a particular sink were within 300 miles of the selected storage location [18].

Energy and GWP impacts associated with the construction of a pipeline network for CO_2 transport were accounted for in this study because anthropogenic CO_2 transport infrastructure does not yet exist at large scale. The initial impacts were annualized, assuming a service life of 30 years. The annualized construction impacts were added to operational use-phase impacts per year. It was assumed that pipes are constructed from commercial steel with a density of 7,900 kg/m^3 with energy consumption of 21.00 MJ/kg steel and GWP of 2.12 kgCO_{2eq}/kg steel, consistent with relevant CCS literature [86]. Pipe diameters were selected using the open-source Integrated Environmental Control Model (IECM) [87], which takes into account several relevant factors; e.g., compressibility, temperature, pressure gradient, average pressure, molecular weight [88]. The model was used to assign nominal diameters for individual pipe stretches of various lengths and anticipated volumetric throughput, based on power plant density in the particular region. Once nominal diameters had been obtained, pipe wall thicknesses were assigned based on the US Code of Federal Regulations (SI section 7). Volumetric throughput (in Mt-CO_2/year) is computed by first summing together the CO_2 emission factors for the membrane-based biogas separation (EF_{mem}) and the power plant flue gas (EF_{PP}), both in units of kg-CO_2/kWh), Equation 3. The sum is then multiplied by the power plant size and nameplate capacity factor (CF). This is necessary to ensure that the biogas quantity will scale to the overall FU, which comes out of the power plant based on its size and utilization [86].

$$Design\ CO_2\ Throughput = \frac{FoS \times (EF_{mem} + EF_{PP}) \times (PP\ Size) \times 8766 \times CF}{1{,}000{,}000} \qquad Eq. 3$$

Carbon storage is achieved via the use of the digestion and post-combustion CO_2 streams for enhanced oil recovery (EOR). Environmental impacts associated with EOR were modeled using the cradle to gate (refinery gate) Oil Production Greenhouse Gas Estimator (OPGEE), developed at Stanford University [89]. This tool computes what amount of CO_2 that can be injected into a particular reservoir and also estimates energy consumption (in units of MJ out/MJ produced crude) and GWP impacts (in units of gCO_2/ MJ crude) for the full life-cycle of oil production and CO_2 and energy factors. The model takes into account specified values of several important reservoir parameters; namely, depth, oilfield gravity, and CO_2 flooding-to-oil production ratio. These properties were collected from databases published by Advanced Resources International (ARI) for all storage locations modeled in this study. Our study uses the default distance of 1.61 km (750 miles) to the refinery gate provided by OPGEE [89]. Correspondingly, the full GWP arising from the combustion of oil produced via EOR was accounted for as part of the A-BECCS life-cycle. It should be noted that there is some variability in how EOR benefits and impacts have been accounted for in previous LCAs [90], [91].

An analysis of this A-BECCS system without oil extraction is also conducted that excludes parameters associated with EOR and instead uses an energy consumption rate of 6.68 kWh/tCO_2 [92].

2.6. Carbon Accounting and Computed Metrics

To summarize from preceding sections, atmospheric CO_2 is taken up into macroalgae biomass via photosynthesis during the cultivation phase. The biomass is then harvested and digested, whereby the organic carbon is transformed and redistributed into several forms during anaerobic digestion, including biogas CO_2, biogas CH_4, digestate liquid (i.e., dissolved organics), and digestate solids (i.e., undigested macroalgae + bacterial biomass). Biogas CO_2 is routed to the EOR location, with some fugitive losses occurring during transport (Section 2.3). Biogas CH_4 is routed to a CHP facility, with some fugitive losses occurring during transport (Section 2.3). Combustion within the CHP facility results in the stoichiometric conversion of bio-CH4 into power plant CO_2, which is then transported to an EOR installation for storage. Fugitive losses also occur during methane storage and power plant CO_2 transport (Section 2.4). EOR is assumed to be a permanent means of sequestering CO_2 (CO_{2geo}), with only 0.09 % losses of methane produced over time [93].

All gaseous losses (CH_4 and CO_2) occurring throughout the A-BECCS life-cycle were assumed to return to the atmosphere. Gaseous CH_4 emissions were multiplied by 12 CO_{2eq}/kgCH_4 to compute the GWP impact based on 100-year GWP values [94]. Fossil carbon impacts were accounted for using GWP impact factors for grid electricity, heat, and other materials consumed during the various unit operations; again, assuming that all gaseous emissions are released to the atmosphere. It was also assumed that all of the carbon in the digestate liquid (ACP) is remineralized to CO_2 during municipal wastewater treatment. In contrast, 54% of the carbon in the digestate solids (SCPS) is permanently sequestered within the municipal landfill. The remainder is converted to CH_4 during solids decomposition, and the CH_4 is flared to produce CO_2, which is then released to the atmosphere (SCP).

Based on the assumed carbon and GWP flows summarized in the preceding paragraph, a net GWP metric was computed according to Equation 4. Fugitive emissions discussed along the supply chain derived from biogas are accounted for ($C_{biogenic\ fugitive\ emissions}$) in net GWP.

$$Net\ GWP = C_{fossil\ fuels} + C_{biogenic\ fugitive\ emissions} + CO_{2\ ACP} + CO_{2\ SCP} - \left(CO_{2\ geo} + CO_{2\ SCPS}\right)\ Eq.4$$

The principal energy metric computed in this analysis was the energy return on investment (EROI). This ratio accounts for energy output (E_{OUT}) as normalized by energy input (E_{IN}).

To better diagnose the performance of A-BECCS additional metrics are needed. The biogenic carbon efficiency is the carbon of biological origin (seaweed or macroalgae) that is permanently sequestered over biogenic carbon released into the atmosphere throughout the life-cycle (from digestion, fugitive emissions from methane transport, aerated liquid digestate, and flared CH_4 from solid digestate in a landfill), or carbon return (sequestered) on carbon investment (CROI) [90]. A hybrid metric that combines net energy use and GHG emissions in units of EJ per GT carbon is also used to compare A-BECCS to other NETs.

3. Results and Discussion

3.1. Visualizing the Scope of A-BECCS

The goal of this study was to quantitatively analyze the energy and climate change impacts of A-BECCS, with a fundamental hypothesis that regional factors would strongly influence its overall performance. Therefore, a valuable first step is visualizing the scope of A-BECCS by mapping its components for each of the three candidate locations. Figure 2 presents this visualization and illustrates what ocean areas are required for macroalgae cultivation within each region. The largest ocean area corresponds to the East Coast (3.06E06 km^2) and area decreases for the West Coast (1.10E06 km^2) and also the Gulf of Mexico (6.57E05 km^2), which relate to regional differences. If the yield were to increase the ocean area and therefore transport distances would also decrease, but in this study, we chose a conservative value and since varying cultivation configurations and biogeochemical factors influence yield it was difficult to accurately represent these differences in the model because of data limitations. Figure 2 also illustrates how power plant (CHP) facilities are distributed throughout each region of interest, to meet the annual power demands in each region. Finally, Figure 2 also shows the location of EOR installations that are used as CO_2 sinks, and more information is found in Section 6 of the Appendix.

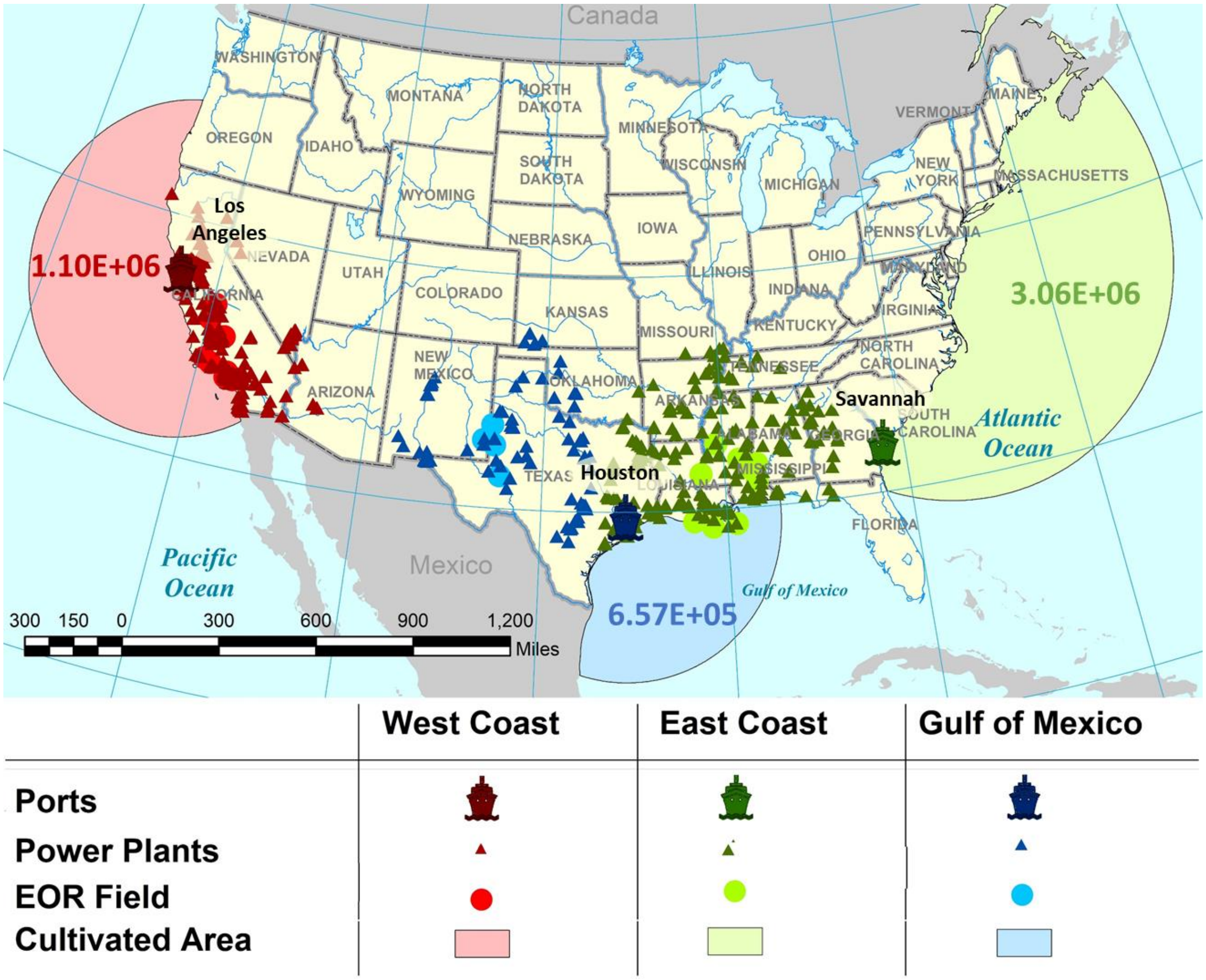

Figure 3. Components of the modeled A-BECCS system mapped onto three candidate locations in the conterminous USA, for visualizing the overall scope of the various life-cycle stages. East Coast (EC) cluster components are shown in green. Gulf of Mexico (GM) cluster components are shown in blue. West Coast (WC) cluster components are shown in red. Ocean regions bounded by the three arcs illustrate what ocean footprint is required for macroalgae cultivation in each modeled cluster. The web version of this article provides color versions of this and other figures.

3.2. Life-Cycle Results: EROI and Net GWP

Given the high complexity of this A-BECCS supply chain (Figure 1) and the expansive geographic scope over which the various processes will occur (Figure 2), it was of interest to evaluate whether A-BECCS could simultaneously achieve net energy production and net carbon sequestration. Accordingly, Figure 4 presents distributions of estimated energy return on investment (EROI) and net global warming potential (GWP) for the three locations of interest. These metrics were computed probabilistically using Monte Carlo simulations, which give rise to distributions of each evaluated output. Table 5 presents means, standard deviations, and other information related to the EROI and net GWP distributions corresponding to each region of interest.

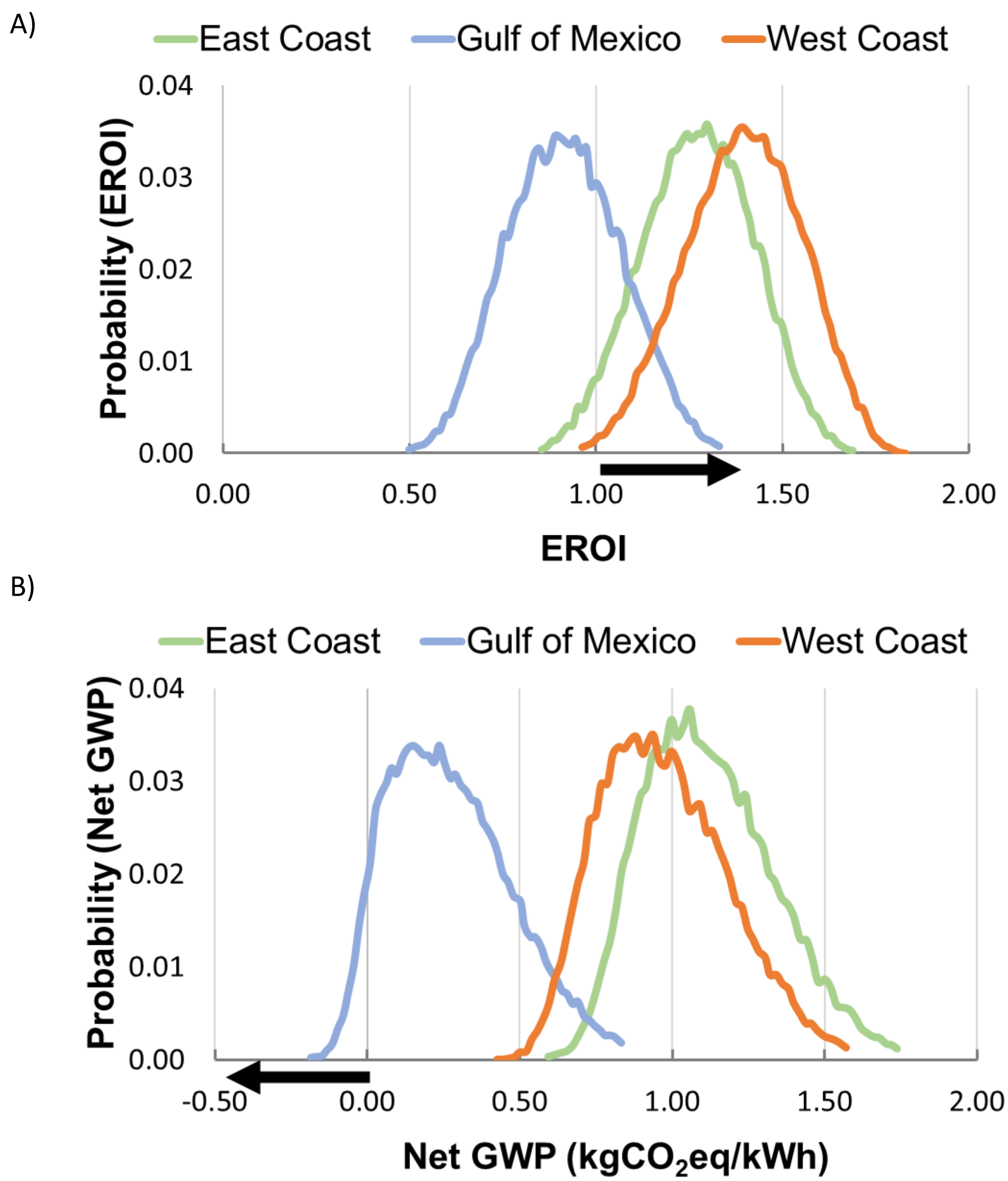

Figure 4. Distributions of metrics for hypothetical A-BECCS systems deployed in three candidate regions of interest. Panel A (upper) depicts energy return on investment (EROI). Panel B (lower) depicts net global warming potential (GWP). Arrows indicate preferred values for each metric; i.e., it is desirable for A-BECCS systems to exhibit EROI >1 and net GWP <0. The web version of this article provides color versions of this and other figures.

Table 5. Summary information for distributions of EROI and net GWP values computed for each candidate location of interest.

Cluster	Mean EROI	Std. Dev. EROI	Prob. EROI>1	Mean Net GWP	Std. Dev. GWP	Prob. GWP<0
East Coast (EC)	1.27	0.15	96%	1.13	0.22	0%
Gulf of Mexico (GM)	0.91	0.15	29%	0.27	0.20	6%
West Coast (WC)	1.40	0.16	100%	0.97	0.22	0%

From Figure 4 and Table 5, it is evident that regionality influences A-BECCS performance. The East Coast and West Coast clusters are fairly similar to each other for both EROI and net GWP metrics, while the Gulf of Mexico cluster is different. Figure 4 and Table 5 also suggest that there is a tradeoff between energy and climate performance for A-BECCS. The East Coast and West Coast clusters exhibit fairly good EROI, such that most of both distributions correspond to EROI >1. However, neither distribution exhibits any probability of net GWP <0. In contrast, the Gulf of Mexico cluster exhibits some likelihood of net negative GWP (6%), but it has a much lower likelihood of EROI >1 (29%). This mismatch reveals that A-BECCS's energy and climate change objectives are not well-aligned when LCA models account for realistic geospatial features.

Although the Gulf of Mexico (GM) system is the only modeled cluster with any likelihood of achieving both EROI >1 and net GWP <0, it is not evident from Figure 4 whether these outcomes occur simultaneously. Therefore, the net GWP and EROI metrics for each trial of the Monte Carlo simulation were plotted against each other. The results are presented in Figure 5. These data reveal that some modeled instances of the GM cluster achieve both EROI >1 and net GWP <0. This situation corresponds to Quadrant IV in Figure 5, which accounts for only about 5% of the total trials. All of the clusters mapped into Quadrants III and IV correspond to net GWP < 0, such that they achieve "negative emissions". Unfortunately, the sum of Quadrants III and IV accounts for only 6% of the total trials. A larger fraction (24%) of trials are mapped into Quadrant II, which exhibits favorable EROI but unfavorable net GWP. Finally, the largest fraction of trials (70%) maps into Quadrant I, which corresponds to poor energy and GWP performances. Accordingly, even though the Gulf of Mexico is the best of the three modeled A-BECCS clusters (Table 5), it exhibits a low likelihood of achieving either EROI >1 or net GWP <0, and its likelihood of achieving both at the same time is extremely low.

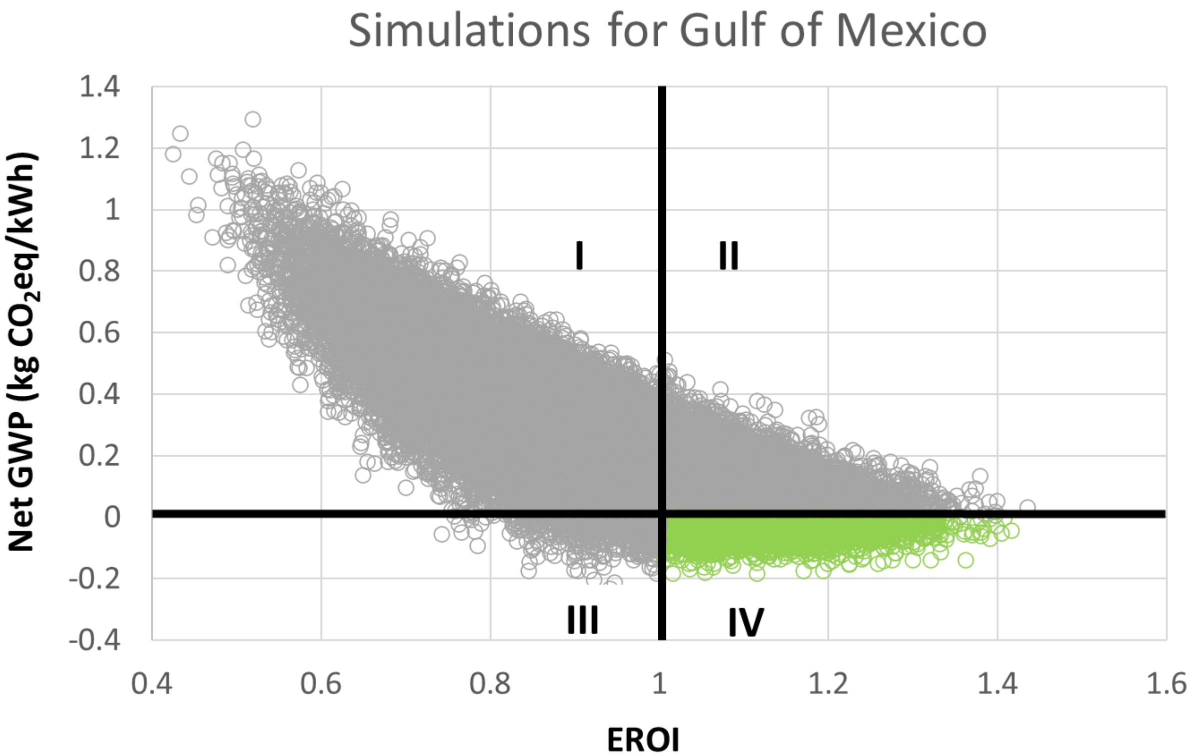

Figure 5. EROI and GWP results of the Monte Carlo simulation (n = 50,000) for the Gulf of Mexico cluster. The fraction of overall trials mapping to each quadrant are as follows: 70% in Quadrant I, 24% in Quadrant II, 1% in Quadrant III, and only 5% in Quadrant IV. The web version of this article provides color versions of this and other figures.

3.3. Diagnosing A-BECCS Challenges

Having observed that the three hypothetical A-BECCS systems offer marginal energy and climate change performances, it is valuable to understand how individual processes affect the energy and carbon impacts of the overall life-cycle system.

3.3.1. Energy Analysis

Figure 6 illustrates the average of data points within the 40-60th percentile of energy production and consumption for all life-cycle stages for each of the three modeled clusters. These data are helpful for understanding which stages of the A-BECCS life-cycle are most problematic, and also for understanding how geography influences the energy performance of each stage. In particular, the results summarized in Figure 6 offer three important observations about how individual life-cycle stages influence the overall energy efficiency of the modeled A-BECCS system.

The first observation from Figure 6 is that biomass procurement is a significant contributor to overall energy consumption in A-BECCS. Algae cultivation and biomass transport (via barge) together account for 33-50% of overall energy consumption across the three modeled clusters. Energy consumption during aquaculture is constant across all clusters and consumes significant energy, and while this is an active research area this trend is seen in other LCAs [17]. Barge transport of wet biomass varies by region and is an outcome of total seaweed needed for the region's power demand, with the Gulf of Mexico having the shortest traveling distance (275 km), and in effect consumes the least amount of energy during barge transport, while the East Coast and West Coast have longer travel distances, 597 km, and 358 km, respectively. Macroalgae aquaculture is an active area of research in the USA, and advancement in more energy-efficient processes and greater yields are expected in the future [16], [24], [93].

The second observation is that energy consumption for digestion is an energy-intensive stage that varies by region ranging from 13-20% of total energy consumption. The variability is a result of differing average port temperature, with the Gulf of Mexico being the warmest (Table 1). Pumping, stirring and heating the digester contribute the most to digestion's energy consumption, and environmental burdens greatly depend on the heat and electricity source. Anaerobic digestion has been previously determined as an energetically intensive process in another LCA study by Langlois et al. (2012) and they also determined that technical and engineering problems resulted in additional energy use [10]. If we compare the CHP energy output (1 kWh) in all cases to digestion, it is consuming >1 kWh, and in the absence of additional energy outputs, this system would be net energy-consuming. It is recommended that alternative bioconversion routes be explored because of both energy consumption and carbon fractionation occurring during digestion, which results in hard to sequester carbon pools, as will be discussed further in section 3.2.1. The biomethane potential of species during digestion is also important in energy production. If anaerobic digestion of macroalgae is still pursued future research should be done in determining macroalgae species' biomethane potentials at bench and pilot scales for species along US coasts since data availability is limited.

Finally, Figure 6 reveals that EOR consumes and produces the most energy (29-52% of total energy consumption depending on region), and without this stage, A-BECCS would not be net energy-producing. The CO_2 injection to oil production ratio is influential for both EROI and GWP and is also known as 'EOR effectiveness' which varies by region (i.e. tCO2 required to extract a barrel of crude). There are tradeoffs with this parameter, the higher it is the less oil being produced and therefore less energy output (EROI decreases), but also results in fewer carbon emissions from recovered oil combustion. The Gulf of Mexico has the smallest magnitude for EOR energy input and output primarily because of this CO_2 injection to oil production ratio parameter. When considering GWP, it is ideal to have a higher ratio, so more CO_2 is being injected than oil is being produced. Since the energy in our system is primarily deriving from EOR this CO_2 to oil production ratio is an influential parameter, and this parameter regionally differs from 0.45, 0.40, and 1.12 for the East Coast, West Coast, and Gulf of Mexico clusters, respectively (distributions are found in Section 6 of the Appendix). In the absence of EOR, the EROI would not be greater than 1. Even though EOR is energy-intensive, the energy output is double that of energy consumed. As discussed, while EOR results in energy output for the system, it also results in large CO_2 emissions which are discussed in section 3.3.2.

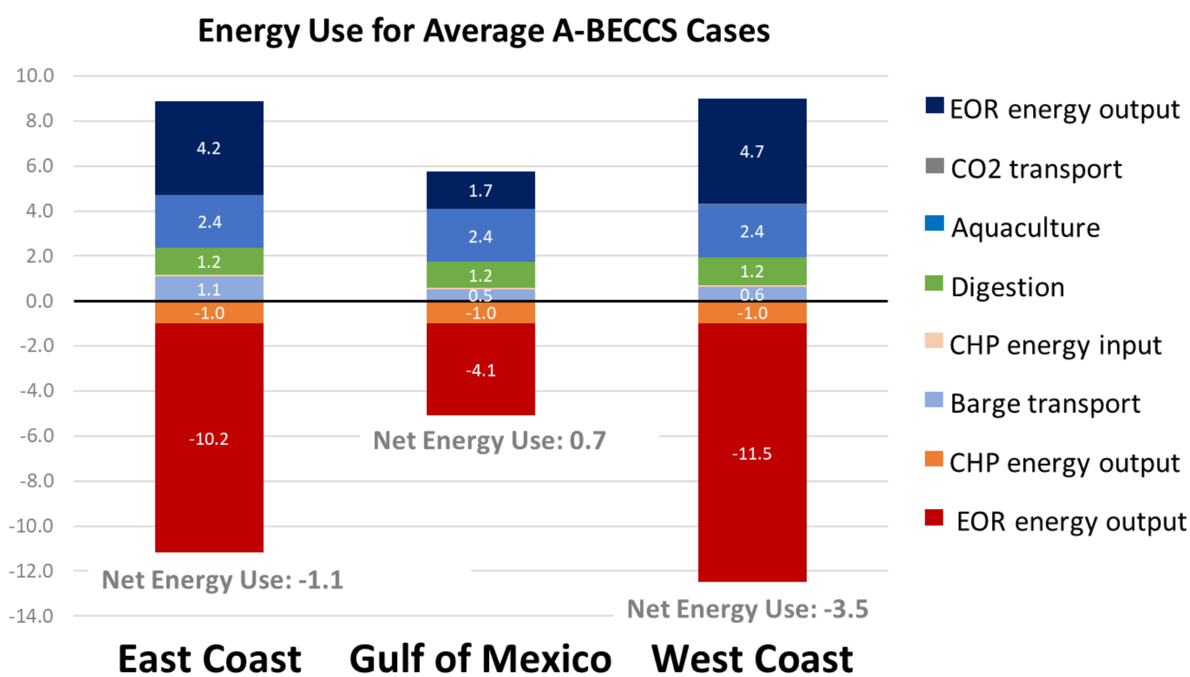

Figure 6. Energy use for each life-cycle stage is quantified for all clusters, and net energy use is labeled at the bottom of stacked bar charts. Negative numbers refer to energy produced while positive refers to energy consumed. The web version of this article provides color versions of this and other figures.

3.3.2. Net GWP Analysis

To determine where carbon is flowing throughout the system it is important to detail these flows in each of the six life-cycle stages. In Figure 7 carbon flows are depicted for the lowest possible GWP or 'best case' extracted from one of 50,000 simulations in the Gulf of Mexico (lowest net GWP trial). Carbon accounting in the system is complex with flows residing in one of four different reservoirs. In Figure 7 the Sankey diagram illustrates biogenic and fossil-derived carbon flows in the system and which of the four reservoirs carbon resides in at the end of the life-cycle. The four different reservoirs include the atmosphere, aqueous waste product, landfill storage, and geological storage. The carbon residing in either the landfill storage or geological storage is effectively stored. The aqueous product is produced from anaerobic digestion residuals and processed through the belt filter press resulting in two waste streams, a solid cake, and an aqueous product. The solid cake is transported to a landfill where 54% of its carbon is effectively stored and the remaining fraction is converted to methane and then flared into the atmosphere as CO_2 [95]. The aqueous product is sent to a wastewater treatment plant where all carbon is assumed to be remineralized as CO_2 and released to the atmosphere.

In Figure 7 we see that in ‘Digestion +’ there are several significant carbon streams from both biogenic and fossil sources that fractionate in all four reservoirs. Processes within ‘Digestion +’ include pretreatment, biogas production, upgrading methane, waste management, and methane transport and storage, which results in a large portion of biogenically sourced carbon being fractionated into pools that are difficult to sequester. This fractionation of carbon necessitates additional waste management processes (e.g. belt filter press and landfilling) and therefore additional energy consumption and greenhouse gas (GHG) emissions. This carbon fractionation resulting from digestion undercuts this system’s negative emission objective. The aforementioned poor energy performance, plus significant technological difficulty (e.g. biological instability, foaming, etc.), makes digestion a problematic bioconversion route within A-BECCS [96]. It would be worthwhile to evaluate alternative bioconversion platforms for macroalgae; e.g., gasification.

In the short term, EOR allows for a smoother transition when deploying negative emission technologies since there is an industrial economic incentive. The USA also has tax credits (45Q) in place for certain CCS projects (including EOR) which makes this CCS configuration economically competitive. But, given the long term goal of deep decarbonization, EOR still contributes significant carbon emissions when oil is combusted, as is accounted for in the model and seen in Figure 7. Several LCAs have applied system boundaries that exclude carbon emissions from the combustion of extracted oil, while our analysis includes carbon emissions from extracted oil combustion [90], [97]. It is therefore philosophically and logistically challenging the modeled A-BECCS system since it is so heavily reliant on fossil fuels to achieve EROI > 1. Even if the oil is not being extracted from these fields there is still some economic incentive with 45Q to geologically store carbon that would also align with decarbonization strategies.

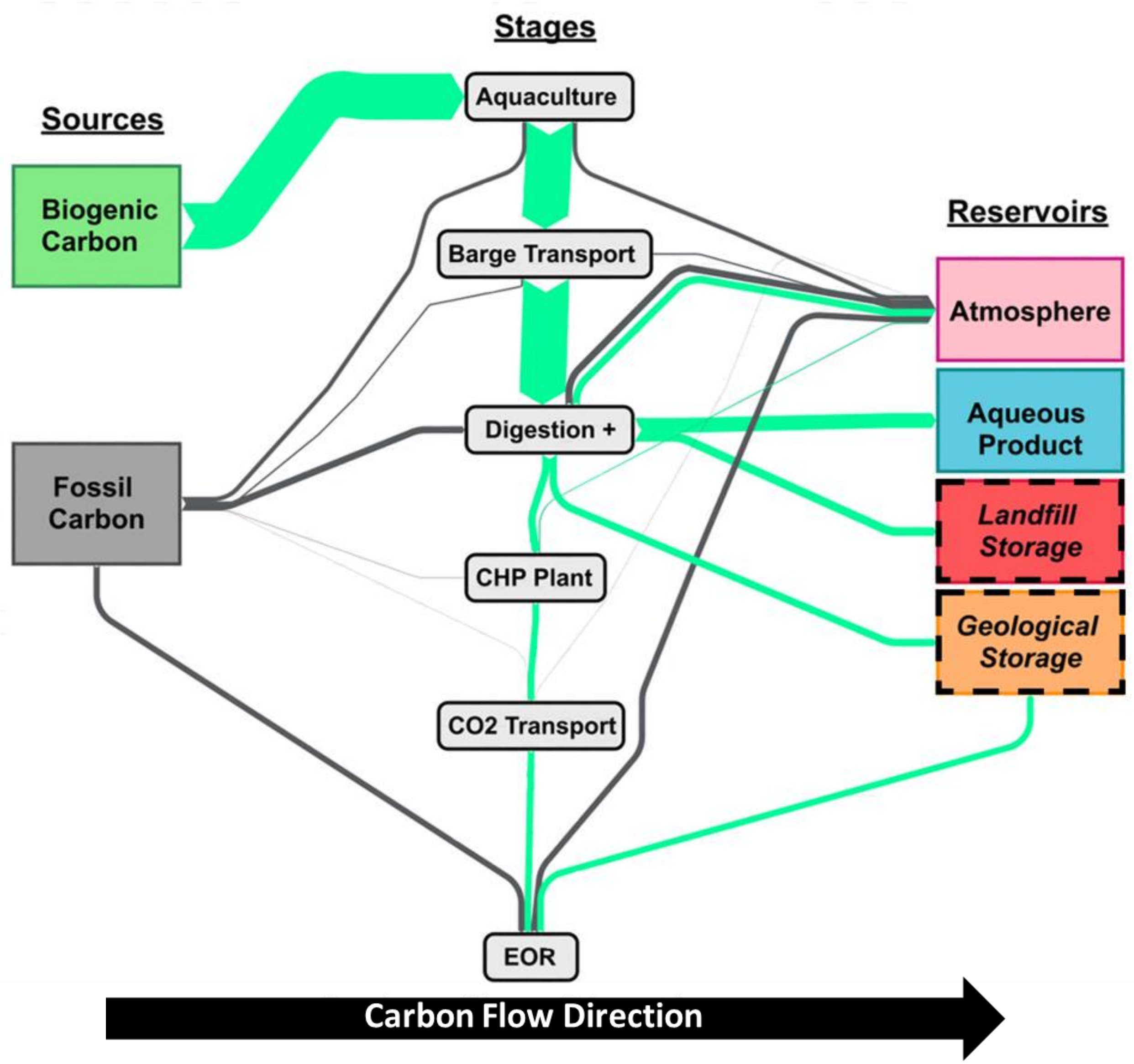

Figure 7. Sankey diagram illustrating all carbon flows from both biogenic and fossil-derived sources, with carbon flows progressing left to right. The carbon resides in one of four reservoirs, where geological storage and landfill storage results in sequestered or stored carbon (italicized and boxed with dashed lines). 'Digestion +' includes pretreatment, upgrading methane, methane transport and storage, and digestion dewatering. The web version of this article provides color versions of this and other figures.

4. Dual Objectives of A-BECCS and System Reconfiguration

The logistic complexities of the system and reliance on EOR to obtain an EROI >1 make A-BECCS incredibly unlikely to meet both objectives (EROI>1 and GWP<0, 5% for the Gulf of Mexico). While EOR was chosen because it was energetically appealing, economically viable, and politically backed it does undermine long term decarbonization strategies. The initial objective of net negative technologies (NETs) was to sequester CO_2 and therefore the focus should be on optimizing CO_2 sequestration over energy production, for there are alternative renewable sources of energy that are available and have greater EROIs than A-BECCS. Therefore, reconfiguring EOR with a focus on increasing carbon sequestration should be considered. In this analysis the carbon emissions associated with oil combustion are significant and in Figure 8 the probability of obtaining a net negative GWP is increased when oil is not extracted from the field and instead the carbon is not utilized and just transported to be geologically sequestered. Also, as discussed, digestion fractionates carbon into several pools making it difficult to sequester while also consuming significant energy. Therefore, A-BECCS should be reconfigured with an alternative bioconversion technology (e.g. gasification), which could result in less energy consumption, is more easily optimized, and creates fewer waste streams.

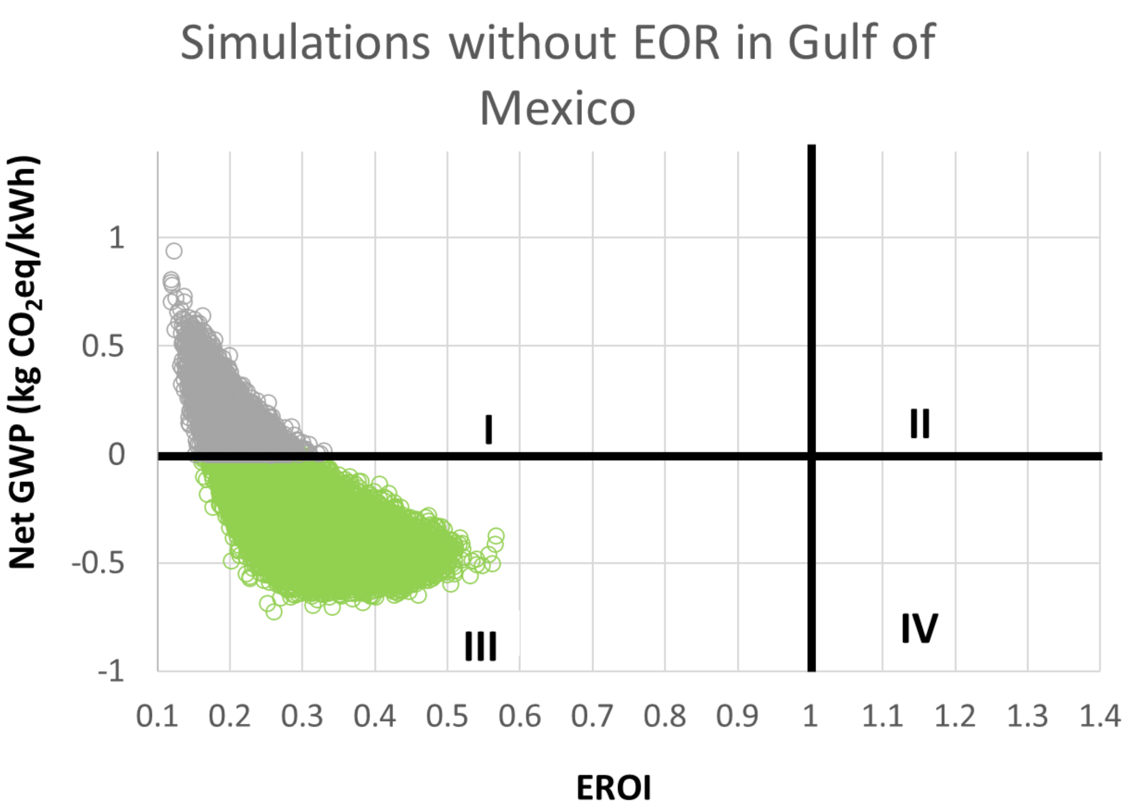

Figure 8. EROI and GWP results for each step of the Monte Carlo simulation (n = 50,000) for the Gulf of Mexico cluster without EOR. With 83% in Quadrant III, EROI<1 and GWP<0. The web version of this article provides color versions of this and other figures.

4.1. Additional Carbon and Energy Metrics

EROI and GWP are not the only metrics that can or should be evaluated. Other metrics have been proposed such as a biogenic carbon efficiency metric by Fajardy et al. (2018), carbon return (sequestered) on [carbon] investment (CROI), and a hybrid metric involving carbon sequestered and energy use to evaluate the system's performance in multiple dimensions and more easily compare it to other NETs [98].
It is difficult to compare A-BECCS to other NETs such as direct air capture (DAC) because boundaries and scope vary significantly and studies are limited, but hybrid metrics can be used to determine how energy-intensive it is per unit of carbon sequestered.

The conversion of macroalgae via anaerobic digestion into bioenergy results in four segregated carbon streams, Figure 7. The biogenic carbon is then more difficult to capture when there are four streams to consider. Most of the biogenic carbon, which is initially up taken by macroalgae via photosynthesis, in the Gulf of Mexico cluster results in sequestration of 49% of photosynthesized carbon that is stored in two streams (landfill and geological storage). This can be termed as a biogenic carbon efficiency metric, or a carbon return on investment (CROI= biogenic sources in kg C sequestered/ total kg C photosynthesized). The resulting 51% of biogenic carbon is released back into the atmosphere from either flaring of methane from solid digestate management in a landfill, and the release of CO_2 from wastewater treatment plants during liquid digestate waste management.

There are limited DAC LCAs and more LCA research of NETs should be done to more accurately compare energy consumption per unit of carbon sequestered. In the Gulf of Mexico's 'best-case,' A-BECCS consumes 25 EJ (net energy) per GT of carbon sequestered while Direct Air Capture (DAC) systems can consume between 47-55 EJ/GT C [2], [97]. For A-BECCS without EOR it is closer to DAC energy use with the 'best-case' scenario consuming 59 EJ per GT of carbon sequestered.

5. Conclusion

The initial conceptual USA based A-BECCS system falls short of delivering net energy (EROI > 1) and sequestering carbon (GWP < 0) effectively. Therefore, a redesign of certain processes within this A-BECCS system where energy and GWP burdens are significant should be researched further. Clusters within the USA that facilitated these conceptual A-BECCS systems resulted in varying environmental burdens because of differences in spatiality. Mapping of NET systems that include supply chain complexities and geographic differences is important in understanding the realities within particular regions and should be further researched. Both digestion and EOR were influential in overall environmental burdens and an alternative bioconversion technology (e.g. gasification) along with a decarbonized geological storage strategy (e.g. deplete oil fields without oil extraction and saline aquifers) should be considered. Prioritizing carbon removal is imperative in optimizing GWP, and considering BECCS's original objective as a negative emission technology, enhanced oil recovery should be reconsidered in future configurations. This system is energy-intensive and while not ideal in its current configuration to meet both objectives, system reconfiguration and optimization could help this NET become viable especially if land use, water use, and food security are a concern.

6. Recommendations for Future Work

Assessing the environmental burdens of entire complex supply chains on a map is necessary to understand these theoretical systems, especially when considering them as a means to mitigate climate change. While most climate target scenarios with NETs implemented assume traditional terrestrial BECCS systems they are scrutinized because of intensive resources us and may not be feasible at the proposed scale. Exploring alternative BECCS systems in which resource use concerns are lessened especially in regards to land use, water use, and food security is a necessary step in finding mitigation pathways for the future, especially when about 39% of Americans live near the coast and energy demand will increase as more individuals move to the coast [99].

This system has marginal energy benefits when EOR is embedded and there is a tradeoff seen between energy production and carbon sequestration. Therefore, a prioritization of carbon sequestration should be considered especially when the goal of a NET is to decarbonize and it is problematic to have this NET supported by oil. Decarbonized storage options for A-BECCS systems such as geologic storage in saline aquifers, which has significant potential in the USA, should be further researched [100]. The system should be redesigned with not only EOR replaced but alternative bioconversion routes that fractionate the biomass into fewer hard to sequester carbon pools should be considered (e.g. gasification). Bioconversion technologies on specific macroalgae species available in the USA should also be experimented on along with determining their optimized harvesting times (e.g. season with highest carbon content). Ocean area is dependent on yield, biomethane potential, and efficiency parameters, and research is currently being conducted and should be furthered in optimizing cultivation configurations (i.e. double lines, the spacing between lines, and fertilization rates) so more accurate modeling is possible to specific regions. There are also multitrophic aquaculture schemes that can decrease fertilizer use with fisheries potentially making this A-BECCS configuration more sustainable. Since significant emissions result from entrained fossil fuel use throughout the stages and research into the option and availability of renewable energy (e.g. offshore wind for aquaculture) should be considered in future studies. NETs within Integrated Assessment Models (IAMs) work under the assumption that they are both socially and economically viable, but not nearly enough research is done within this sphere and should be done in the future for this and other NETs [101]. This is the first regionally explicit A-BECCS study making this topic ripe with further research opportunities.

7. Products of this thesis

- Interned at the *Department of Energy* in the Office of Environmental Management from June 2019-August 2019.
- One of 40 students accepted into the *Carbon Capture and Storage Summer School hosted by the International Energy Agency* from July 7-13, 2019. A poster was also presented.
- Poster presentations at conferences: 2018 *American Geophysical Union (AGU)* Fall Meeting, and 2019 *Carbon Capture, Utilization and Storage Gordon Research Conference (CCUS)*
- **Awards:**
    - UVA Engineering Dean's Scholar Fellow, University of Virginia, August 2018-May 2020
    - Graduate Assistantships in Areas of National Need Fellow, US Department of Education, August 2017-August 2018
    - HSF Scholar, Hispanic Scholarship Fund, August 2019-May 2020

Competing interests

None

Acknowledgments

GAANN P200A160322, UVA Engineering Dean's Fellowship

Appendix

Table of Contents

1. Model Overview

In this study, life-cycle assessment (LCA) is used together with a GIS (geographic information system) framework to estimate the environmental impacts of aquatic bioenergy with carbon capture and storage (A-BECCS) at three locations in the conterminous United States. The A-BECCS system modeled in this analysis includes the following main processes: aquaculture, biomass transport, fuel generation, bio-electricity generation, CO_2 transport, and use of CO_2 for enhanced oil recovery (EOR). It is assumed that cultivation, harvesting, and biomass transport occurs offshore in the ocean, while all other processes are performed on land.

1.1. Functional Unit and Computed Metrics

The functional unit (FU) for this analysis is annual power generation for each modeled case, as normalized to 1 kWh. Energy and climate change impacts are quantified using several relevant metrics. The principal energy metric is energy return on investment (EROI). This ratio encapsulates energy output (E_{OUT}), as normalized by energy input (E_{IN}). The principal climate change metric is net global warming potential (GWP), in units of kg CO_2-equivalents/FU, based on 100-year GWP values from the IPCC's Fifth Assessment Report [102]. An additional efficiency metric is also computed to articulate interactions within net carbon sequestration, and can then be compared to other BECCS systems [98]. We compute a biological carbon sequestration efficiency metric which we refer to as carbon return on [carbon] investment (CROI); i.e., kgCO_2 sequestered / kgCO_2-eq emitted [98]. A hybrid metric is also computed to understand the energy consumption, in units of kWh, per GT of carbon sequestered, which can then be compared to various NETs.

1.2. Modeled Clusters

Three coastal regions in the conterminous US are evaluated using the LCA-GIS framework, namely: East Coast, Gulf of Mexico, and West Coast. Relevant geographic regions for these clusters are illustrated in Figure 3 of the paper, and an overview of the modeled processes corresponding to each cluster are described in section 2.1 of the paper.

2. Aquaculture

2.1. Aquaculture Overview

The large scope of A-BECCS operations required to achieve climate change mitigation goals will necessitate the purposeful cultivation of marine biomass rather than relying on naturally occurring stocks. This analysis, therefore, assumes that current best practices from commercial aquaculture are adopted for use in producing A-BECCS feedstocks[103]–[107]. In particular, this study focuses on aquaculture systems in which macroalgae are cultivated offshore on 100-meter-long lines (ropes) (Figure A1). A conservative yield was used based on the assumption that lines are 5 meters, 100 m long and 20 long lines, with vertical hanging lines carrying seaweeds every 50 cm per hectare apart from each other, with research efforts on line configurations and yield are underway [108]–[110].

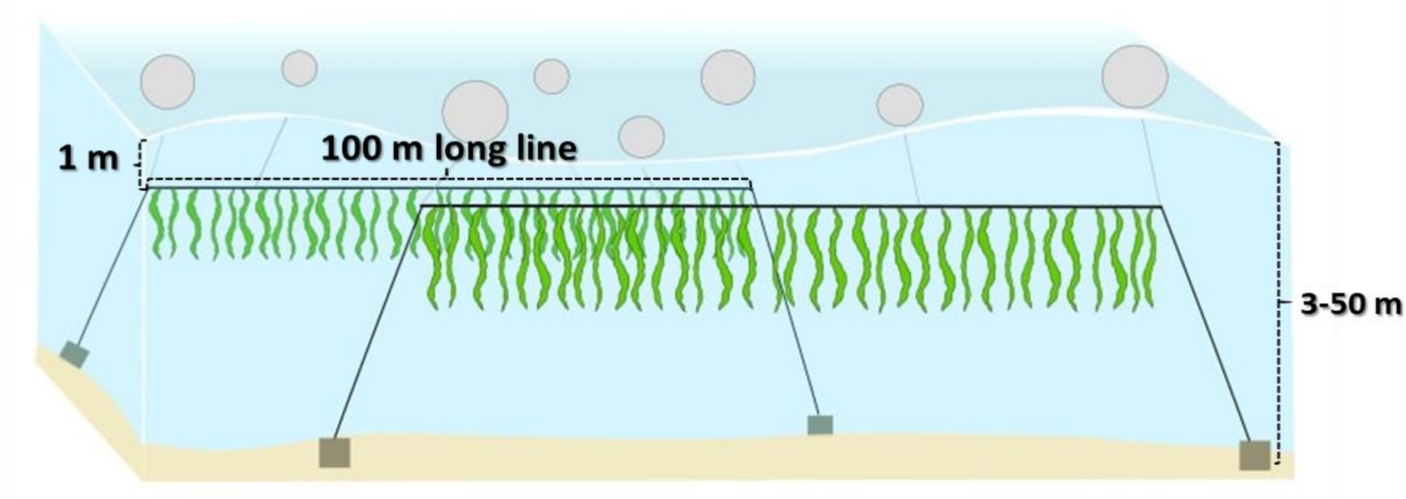

Figure A1. 100-meter-long lines are tethered at least 1 meter below surface waters at depths that vary from 3-50 meters and are supported by buoys at the surface. Diagram created was adapted from Edwards et al., 2011 and Czyrnek-Delêtre et al 2017.

Current commercial aquaculture relies on three kinds of macroalgae (i.e., seaweed or kelp), which are categorized based on pigmentation: brown (e.g., *Laminaria spp., Sargassum spp., Undaria spp*.), red (e.g., *Eucheum spp*., *Gracilaria spp*., *Porphyra spp*.), and green (e.g. *Enteromorpha clathrate, Monostroma nitidum, Caulerpa spp*.) [111], [112]. Growth of these strains is modulated by environmental conditions (e.g., insolation, temperature, salinity, etc.) such that individual strains exhibit different growth by region [112], [113]. For this analysis, it is assumed that all three geographic locations are producing a hypothetical mixture of brown macroalgae that principally includes *Saccharina latissima*, *Laminaria digitata, Sargassum muticum,* and *Macrocystis pyrifera*, as discussed in section 2.2 of the manuscript. Elemental composition and other feedstock parameters for this hypothetical mixture are summarized in Table 2 of the manuscript. Lack of data made it impossible to parameterize the differences in feedstock grown for different geographic regions.

2.2. Cultivation Phase

Parameters and assumptions for energy use and CO_2 during the nursery and open ocean cultivation phases were collected from Alvarado-Morales et al. (2013) and are outlined in Table A1. Spore collection is not accounted for in this study since energy and GWP are negligible during this process. Once kelp spore growth is sufficiently well established, kelp is transported on lines out of the nursery and transplanted into the ocean [104], [114]. The kelp is then cultivated on long lines for approximately five months [105]. During this time, maintenance and observation are required at a rate of one visit per month which is also accounted for by Alvarado-Morales et al. [114].

Table A1. Parameters and assumptions used from Alvarado-Morales et al.

Input	Units	Min	Likely (Median)	Max	Distribution
CO_2 emission factor for nursery, cultivation, harvest	kg CO_2/ kgTS	0.10	0.11	0.12	Triangular
Energy consumption rate during nursery, harvest, and cultivation	kWh/kgTS	0.54	0.59	0.65	Triangular
Fertilizer consumption during nursery	kg /kgTS	-	1.89E-04	-	-

Specific fertilizer quantifications used during the nursery phase were not explicitly stated and were assumed based on a subsample of nitrogen (N) and phosphorous (P) elemental composition ratios within one standard deviation of the mean. The N/P ratio was assigned a triangular distribution with the likeliest ratio being 7.92 (N:P), maximum= 8.69 and minimum= 7.15; the data for N/P averages were mainly from *Saccharina latissima* and *Laminaria digitata* samples and similar nitrogen and phosphorous percentages were found in *Sargassum muticum* and *Macrocystis pyrifera* [40], [40], [48], [115], [116]. Then, fertilizer is again applied during the ocean grow-out phase, and consumption during this phase is computed based on the elemental composition of the kelp used to compute ratios. On one hand, this approach may underestimate true fertilizer demand in so far as it assumes that all fertilizer is taken up by the kelp and that none is consumed by competing reactions (e.g., taken up by other organisms) or transported out of the growing zone. On the other hand, this approach may overestimate true fertilizer demand in so far as it does not account for background ocean concentrations of N and P (usually 30 µmol/kg and 2 µmol/kg), in the circulating ocean waters [117]. It was decided that these competing factors may essentially cancel each other out, such that it is valid to compute fertilizer demand based on kelp's elemental composition, therefore a factor of safety was assigned to a uniform distribution over the range 0-2, corresponding to 0-100% stoichiometric excess.

While our model could not account for regional factors affecting kelp cultivation in the open ocean cultivation phase, there is research that supports our rationale for choosing our hypothetical mix and assures that chosen species can be successfully cultivated along US coasts [103], [106], [113], [118]. Ideal sea surface temperatures for brown macroalgae are within 10-16^{o} C, with higher latitudes offering better growth year-round [113]. While optimal photosynthetically active radiation (PAR) is higher in lower latitudes, which includes solar wavelengths between 400 and 700 nm and can be reclassified into various suitability ranges in units of moles/m^2-d (<2.6 unsuitable and ≥6.9 high suitability)[113]. Within the US exclusive economic zone (EEZ is 1.85 km off the coast) the Gulf of Mexico has the highest suitability throughout most of the year (PAR >6.9 moles/m^2-d), while the east and west coast have medium to high suitability throughout the year (PAR ≥ 4 < 6.9 moles/m^2-d) [113].

2.3. Harvesting and Transport

For currently operating commercial aquaculture facilities, kelp is produced in relatively small farms that are located close to shore, and harvesting is performed manually. However, it is anticipated that the large scope of A-BECCS operations will make it necessary to cultivate kelp farther offshore and making use of mechanized harvesting. After harvesting the biomass it is transported via barge, to a coastal port [108], [113]. Energy and GWP impact factors for barge transport are in section 2.2 of the manuscript [119]. There is limited data on energy consumption and GWP for a seafaring barge but is assumed to be comparable to inland water operated barges. The weight transported is computed based on the dry weight of feedstock required to deliver 1 FU (see Section 2.4 of the manuscript and SI section 3.3) and the water content of the kelp. In this analysis, water content for freshly harvested macroalgae is assigned to a triangular distribution, with likeliest = 81.50 % FW (Table 1 of main manuscript). The use of logic statements was undesired and therefore an artificial maximum on water content for macroalgae was set to 85%, since digester water content was assumed to be 85% (section 2.3 of manuscript).

3. Anaerobic Digestion

It is assumed that the kelp feedstock is pretreated and then anaerobically digested to produce biogas, which is then used to create bio-electricity.

3.1. Pretreatment

No significant dewatering is required during pre-treatment since the water content of the pretreated biomass is directly suitable for low solid (or wet) mesophilic anaerobic digestion. The total solids content of pretreated biomass is 10%, and kelp feedstock satisfies the low solid digestion feedstock typically required, ≤ 15 % TS (moisture content ≥ 85% FW) [114], [120], [121].

3.2. Ensiling [Excluded from Model]

Some preliminary A-BECCS literature refers to biomass storage and a pre-processing step referred to as ensiling [122]–[124]. This step can be useful for managing seasonal variability in feedstock availability and ultimately ensuring that the CHP facilities have continuous fuel stockpiles accessible.

Before ensiling, the macerated (pretreated) algae feedstock (Section 3.1) is dewatered to achieve moisture content less than or equal to 75% [125]. Typical water contents for relevant macroalgae strains range from 75-89% (Table 2 in manuscript), which can make drying very environmentally burdensome in some cases. The feedstock is then stored under anaerobic conditions for long durations (e.g., up to 6 months). During this time, fermentation reactions occur, thereby converting some feedstock carbohydrates into organic acids, which results in low pH conditions that help to preserve the macroalgae [110]. The preliminary fermentation reactions also consume a small fraction (2.5-3.1%) of initial feedstock volatile solids (VS) [126], [127]. After ensiling is completed, the silage is diluted with fresh water to achieve a moisture content of ≥ 85%, such it is then suitable for anaerobic digestion.

The literature does not clearly articulate what impact ensiling has on anaerobic digestion. Various studies report mixed effects on biomethane potential (BMP), which is the volume of methane that is produced per mass of feedstock digested (Section 2.3 in manuscript and 3.3 in this SI) [121], [122], [126], [128], [129]. In these studies, methane output for ensiled feedstock increases, decreases, or stays the same compared to controls without ensiling. Therefore, based on current data, ensiling appears to dramatically increase energy use, GWP, and water consumption for BECCS without conferring any appreciable increase in energy output or sequesterable CO_2. For this reason, ensiling is excluded from this analysis, and it is assumed that CHP facilities make use of biogas stockpiling instead of feedstock storage to ensure adequate, uninterrupted fuel supply (Section 4).

3.3. Biogas Production

The anaerobic digester is modeled as a continuously stirred tank reactor operated under mesophilic conditions (average temperature= 35^0C) [125], [130]. Previous work suggests that there is no appreciable difference in methane output between mesophilic and thermophilic conditions, while mesophilic digesters consume less energy for heating compared to thermophilic digesters [131]. Organic loading rates, solids retention times, and biodegradability (i.e., the fraction of volatile solids removed during treatment) under these conditions are given in Table 3 of the manuscript.

It is noteworthy that all A-BECCS operations modeled in this study are scaled based on digester output, insofar as anaerobic digestion forms the link between biomass cultivation and bio-electricity production, and the FU for this analysis is 1 kWh of net bio-electricity production. In particular, the efficiency of methane production during anaerobic digestion modulates the scale of all upstream and downstream processes for the production of 1 kWh because it influences how much biomass is consumed and what amount of product gases are created. Section 2.4 of the manuscript and Equation 2 describes how the mass of methane required to produce 1 FU is computed. The approach that is used takes into account methane energy content and several efficiency parameters for CHP facilities performing carbon capture and storage (CCS).

The fugitive emission rate and distribution from digestion (L_{AD}) are given in Table 3 of the manuscript. Our study is assuming a well-managed and operated digester, which should be comparable to the maximum fugitive loss seen in a natural gas plant [76], [77].

Once the total required mass of methane per FU has been computed, it is then possible to determine what amount of macroalgae feedstock is required. This quantity is calculated using the biomethane potential (BMP), which represents the volume of methane produced per mass of volatile solids (VS) biodegraded during anaerobic digestion. Typical units of BMP are ml CH_4/kg VS, and are converted to m^3/g VS in our model (normal temperature and pressure, 20^0C and 1 atm). Table A2 presents BMP values gleaned from literature for various relevant macroalgae species digested under mesophilic conditions in the interested regions. The maximum and minimum BMP values assigned to the triangular distribution is taken from a subset of data within one standard deviation of the mean of collated BMP values. The BMP range reflects significant variability in methane yield arising from variability in feedstock biochemical composition, which changes with cultivation conditions (e.g., depth, harvest season), and also digestion parameters (e.g., temperature, solids retention time, pH, etc) [132]–[135]. Finally, as noted in Section 2.1, there is not currently enough data available to parameterize differences in BMP for macroalgae production in different locations. Therefore, the same BMP distribution is used for all three selected geographic regions.

Table A2. Biomethane potential of various brown macroalgae species under mesophilic conditions

Biomethane Potential (m^3/gVS)	Species	Source
1.87E-04	*Laminaria digitata*	[76]
9.34E-05	*Laminaria digitata*	[44]
2.09E-04	*Saccharina latissima*	[44]
1.67E-04	*Laminaria digitata, Saccharina latissima and Laminaria hyperborea*	[42]
2.08E-04	*Saccharina latissima*	[79]
1.57E-04	*Saccharina latissima*	[79]
1.20E-04	*Laminaria digitata, Saccharina latissima and Laminaria hyperborea*	[56]
3.42E-04	*Laminaria digitata, Saccharina latissima and Laminaria hyperborea*	[56]
2.20E-04	*Laminaria digitata, Saccharina latissima and Laminaria hyperborea*	[56]
2.88E-04	*Laminaria digitata, Saccharina latissima and Laminaria hyperborea*	[56]
2.96E-04	*Laminaria digitata, Saccharina latissima and Laminaria hyperborea*	[56]
3.38E-04	*Laminaria digitata, Saccharina latissima and Laminaria hyperborea*	[56]
3.02E-04	*Laminiaria digitata*	[78]
2.81E-04	*Saccharina latissima*	[78]
2.98E-04	*Laminaria digitata*	[78]
3.43E-04	*Laminaria digitata*	[78]
3.30E-04	*Laminaria digitata*	[78]
2.25E-04	*Sargassum muticum*	[32]
1.77E-04	*Sargassum muticum*	[32]
1.85E-04	*Sargassum muticum*	[45]
1.50E-04	*Sargassum muticum*	[45]
1.95E-04	*Sargassum muticum*	[45]
1.55E-04	*Sargassum muticum*	[45]
2.10E-04	*Sargassum muticum*	[45]
2.05E-04	*Sargassum muticum*	[45]
1.30E-04	*Sargassum muticum*	[14]
4.30E-04	*Macrocystis pyrifera*	[48]
2.39E-04	*Macrocystis pyrifera*	[46]
2.62E-04	*Macrocystis pyrifera*	[46]
1.77E-04	*Macrocystis pyrifera*	[46]
2.78E-04	*Macrocystis pyrifera*	[46]

To compute the fresh weight biomass ($Biomass_{FW}$) of macroalgae required to deliver 1 FU, the required methane mass is first computed which is then divided by the BMP [in kg CH_4/ g VS] using the density of methane 0.66 kg/m^3 (at 20 °C, 1 atm)[136]. The resulting quantity then multiplied by the VS/TS ratio given in Table 2 in the main manuscript (ash-free dry weight [AFDW] fraction). The AFDW adjustment is necessary to account for the presence of inert, non-digestible material (i.e., "ash") in the raw feedstock since only VS can be converted into CH_4. The AFDW fraction is then given by 100% minus ash content. It is equivalent to the ratio VS/TS, where TS is total dry solids. From literature, ash content is assigned to a uniform distribution ranging from 554-758, Table 2 in the manuscript. The resulting feedstock mass corresponds to the dry weight or Total Solids ($Biomass_{TS}$) of macroalgae required to deliver 1 FU. This quantity can be converted to a raw wet weight basis, if necessary, using the water content as seen in Equation A1.

$$Biomass_{FW}\left\{\frac{kg}{kWh}\right\} = Biomass_{TS}\left\{\frac{kg}{kWh}\right\} \div \left(1 - \frac{Water\ Content\ \{\%\ FW\}}{100}\right) \qquad Eq. A1$$

Finally, just as BMP varies in response to changes in feedstock composition and digestion operating conditions, so does the fraction of CH_4 in the biogas. Methanogenic organisms in the anaerobic digester produce both CH_4 and CO_2 together during biodegradation, so both are always present in the biogas. Table 3 in the main manuscript summarizes CH_4 biogas fractions from literature, but literature reporting BMP values do not always report methane percentage therefore matching BMP to methane percentages is difficult. For modeling purposes, a subset of this data within one standard deviation of the mean is assigned to a triangular distribution with the likeliest value = 47.3% (vol/vol), in Table 3 [137]–[139]. It is assumed that the remaining fraction of the biogas constitutes CO_2.

3.4. Digestion Inputs: Electricity Use and Heating

Mesophilic anaerobic digestion (35°C) consumes significant electricity and heat. In this analysis, electricity consumption quantities are estimated using an empirical regression equation developed by Soda et al. and based on mesophilic anaerobic digestion operations at municipal wastewater treatment plants [131]. While heating is regionally specific and is estimated using the specific heat of the water content and is given in Equation A1.

3.5. Belt-Filter Pressing

A belt filter press (BFP) is used to dewater the wet digester residuals ("digestate") to facilitate their transport and disposal. Liquid digestate is transported to a wastewater treatment plant, while solid digestate is transported to a well-managed landfill. Electricity consumption for this process is computed using an empirical equation from Soda et al. [131]. This expression takes the form of Equation A2, where W is BFP electricity consumption in kWh/tonne TS. X is equal to 40 tonnes TS per day because the original formulation was calibrated over a range of sludge loading weights with that maximum value. Digestate was not used as fertilizer because of high salinity, possible accumulation of heavy metals, and the ongoing debate of its benefits for traditional agriculture [140], [141].

$$W = -110\ln(x) + 540 \qquad Eq. A2$$

BFP electricity consumption is multiplied by the mass of digestate residuals arising from anaerobic digestion, which is equal to the total mass of feedstock required per FU (Section 3.3) minus the fraction that is biodegraded during digestion. Assumed biodegradability is 58% (see Section 3.3) to compute total digester electricity consumption per FU. It is assumed that this electricity comes from the US regional grid.

3.6. Biogas Upgrading and Pressurization

The biogas produced during anaerobic digestion constitutes a mixture of CH_4, CO_2, and various trace gases. It is beneficial to remove the trace gases (e.g., H_2S) and water vapor. To get a more purified methane and CO_2 stream these gases must be separated. In this analysis, it is assumed that pressure swing adsorption (PSA) is used to separate the main biogas constituents, CO_2 and CH_4. PSA is a widely used biogas separation technology, in which pre-conditioned, compressed biogas is fed into a column with an adsorbent that selectively retains CO_2 (e.g., carbon molecular sieves, zeolites, etc.). The CH_4 passes through and is collected as a purified stream [78], [142]. Over time, the adsorbent material becomes saturated with CO_2 and must be regenerated. This is done by decreasing the pressure dramatically (e.g., to vacuum) such that the CO_2 can be evacuated. The loading and unloading then continue cyclically. A schematic is included for clarification and percentages of gas streams, Figure A2.

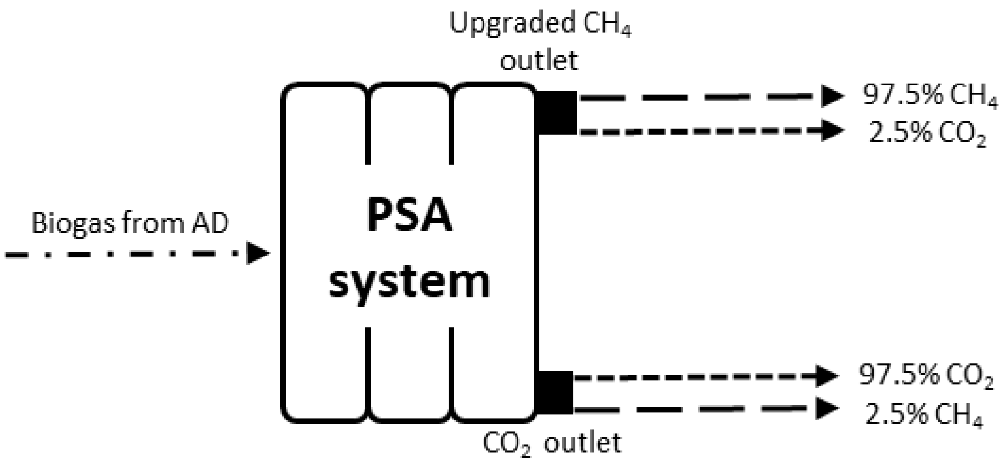

Figure A2. Schematic of PSA system and gas streams

It is unclear if the energy consumption includes the removal of minor gases (i.e. H_2S), but this study assumes so. The total volume of biogas corresponding to 1 FU is given by methane volume per FU [in m^3] divided by the methane fraction in the biogas. A 2.5% loss of produced methane is usually seen in the pressure swing adsorption (PSA) system used to separate CO_2 from CH_4 and is accounted for and assumed to be in the stream that is predominately CO_2, Figure A2 [78].

4. CHP Facility Operations

4.1. Fuel (Methane) Storage and transport

It is standard practice for coal power plants in the US to maintain at least 60-90 day supply of fuel on-site, while natural gas is typically stored underground [71]. In this analysis, it is assumed that methane is separated from digester biogas, compressed, and then transported to an on-site storage location at a CHP facility. Electricity consumption for pressurization at the storage location is 6.5 kWh/tCH_4 [143]. It is also assumed that methane leakage during storage (L_s) is 0.36% of methane transported, data from The Greenhouse Gases, Regulated Emissions, and Energy Use in Transportation Model (GREET) [80].

4.2. Power generation

The mass of methane required to produce 1 kWh of electricity in a CHP facility is computed using Equation 2 of the manuscript and takes into account the energy penalty for CCS. In the

CHP power plant, an energy penalty associated with compressing the CO_2 captured is accounted for in Equation A3 (Energy Penalty_{CCS}). Energy_{CC} is the energy required for compressing CO_2 to 14 MPa, and assigning a triangular distribution to the CO_2 capture rate with likeliest= 90% (CR), minimum= 75% and maximum= 90%. The heat generated from the CHP plant is directly used for monoethanolamine (MEA) sorption of CO_2 [144].

$$Energy\ Penalty_{CCS}\{kwh\} = Energy_{CC}\left\{\frac{kWh}{kgCO_2}\right\} \times CHP\ emissions\left\{\frac{kg\ CO_2}{kWh}\right\} \times CR \qquad Eq. A3$$

The thermal electrical equivalent (Q_{TEE}) was calculated by rearranging the Effective Electric Efficiency that allows comparison of a CHP to conventional power systems (e.g. natural gas-fired broiler) [145]. In Equation A4, Q_{TEE} was computed using both electrical and thermal efficiencies and using the efficiency of a natural gas broiler (λ=.80) which would have been the conventional technology that otherwise would be used to produce the useful thermal energy output if the CHP system did not exist [145]. The energy required during the CO_2 sorption phase after energy generation is supplied by the heat created by the CHP plant. The thermal electrical equivalent allows us to determine the useable amount of heat recycled from the power plant in Equation A5. The useable heat leftover after absorption is calculated using Equation A5 and is around 350-500 kJ/ kWh for different regions and accounted for as an energy output for EROI.

$$Q_{TEE}\left\{\frac{kWh}{kWh}\right\} = \frac{\left({}^{\eta_{TE}}/_{\eta_{EE}} - 1\right) \times \lambda}{\lambda - \eta_{TE}} \qquad Eq. A4$$

$$Q_{Therm}\left\{\frac{KJ}{kWh}\right\} = \left(Q_{TEE}\left\{\frac{kWh}{kWh}\right\} \times \frac{3600\ KJ}{kWh}\right) - \left(CO_{2_{CHP}}\left\{\frac{kgCO_2}{kWh}\right\} \times Heating_{MEA}\left\{\frac{KJ}{kgCO_2}\right\}\right) \quad Eq. A5$$

The CO_2 captured in the CHP plant is calculated by converting the volume of methane after going through the PSA system into mass (kg/kWh) which is then combusted in the CHP plant and converted to CO_2, and multiplying by the CO_2 capture rate, Eq A6. The conversion of CH_4 to CO_2 was done by dividing through by the molecular weights. The CO_2 not captured by the PSA system (2.5%) is accounted for in the volume of methane going into the CHP plant.

$$CO_{2_{CHP}}\left\{\frac{kg}{kWh}\right\} = CH_{4_{PSA}}\left\{\frac{kg}{kWH}\right\} \times \left(\frac{16\ \frac{g}{mol}}{44\ \frac{g}{mol}}\right) \times CR\{\%\} \qquad Eq. A6$$

5. Direct and Indirect Carbon and GHG Accounting

Biological CO_2 uptake is computed as the product of feedstock mass required to produce 1 FU and the macroalgae's carbon content (Table 2 in the manuscript). The carbon content reflects spatial and temporal variety, insofar as feedstocks cultivated in different locations exhibit some variability in carbon content. Feedstock produced in a single region also exhibits appreciable seasonal variability, typically with higher values in summer and lower values in winter[135], [146]. Since data is limited, we could not parameterize our model to reflect this variability.

Conversion of carbon to CO_2 was done by dividing the molecular weights of CO_2 and carbon (CO_2=44 g/mol, C=12 g/mol). To calculate how much carbon is sequestered biologically the amount of biomass needed per FU must first be known and it is calculated using Equation A1, and Equation 2 in the manuscript. First, the mass of methane needed to produce 1 kWh is calculated, which uses biomethane potentials (BMP) from literature, and accounts for losses in bio-methane along the supply chain (i.e anaerobic digestion), and power plant efficiencies.

$$Carbon\ uptake \left\{\frac{kg\ CO_2}{kWh}\right\} = Biomass_{TS}\left\{\frac{kg}{kWh}\right\} \times Carbon\ Content\ \{\%\} \times \frac{44\ \frac{g}{mol}}{12\ \frac{g}{mol}} \qquad Eq. A7$$

One must also consider the carbon in both the liquid and solid digestate. The solid from the BFP will be landfilled and some studies have considered how much of that carbon is remineralized after being landfilled over 100 years. This study assumed 46% of the carbon landfilled will be emitted as CO_2 (after flaring) while the rest is permanently stored [147]. All carbon resulting in the atmosphere from biogenic sources is accounted for. Biological carbon sequestered goes into 4 different reservoirs: atmosphere, aqueous product, solid cake, or geological storage as described in Section 2.6 in the manuscript.

6. CO_2 Transport Networks: Mapping Source-Sink Pairings

Transport distance is a critical parameter for assessing the feasibility of A-BECCS in the context of realistic biophysical and geospatial features. For this study, it was assumed that CO_2 sequestration would occur at locations that are suitable for CO_2 use in enhanced oil recovery (EOR). A previous analysis by Abotalib et al. (2016) evaluated CO_2 injection for EOR applications in five US regions: Permian Basin, Gulf Coast, Rockies, Mid-Continent, and California basins [18]. Three of these five (Permian Basin, Gulf Coast, and California Basin) are evaluated in this study. The other two (Rockies and Mid-Continent) were excluded because it was presumed that they are too distant from the coast to be practically workable for A-BECCS.

A network of transport lengths was created based on the mapping of prospective source and sink locations in each of the three storage basins of interest. Methodologies for each basin are described in the following sub-sections. It is emphasized that the spatially-explicit source/sink mapping was focused on future CO_2 transport instead of present CO_2 throughout.

California

For compiling the locations and geologic properties of suitable EOR sites, we largely relied upon studies by ARI, which concluded that EOR-relevant locations are located predominantly in Southern California [82]. It was therefore decided that only Southern California reservoirs would be included in the current study. These locations are summarized in Table A3. For ease of analysis, transport distances were computed assuming that the pipeline runs to the Euclidean center of each storage reservoir (Figure A3). This value was applied to all locations in Table A3.

Table A3. Reservoirs having EOR potential in California as listed by ARI [82]

Reservoir	Depth (ft)	Oil Gravity (API)	Basin Name	Longitude	Latitude
Elk Hills (Stevens)	5500	35	San Joaquin Basin	-118.86	35.49
Coalinga, E. Extension (Nose Area)	7800	30	San Joaquin Basin	-119.78	36.73
Kettleman, N. Dome (Temblor)	8000	36	San Joaquin Basin	-119.88	36.09
Cuyama S. (Homan)	4000	32	San Joaquin Basin	-119.69	34.42
Elk Hills (Main Area/Upper)	3000	22.5	San Joaquin Basin	-118.86	35.49
Fruitvale (Etchegoin-Chanac)	3730	19	San Joaquin Basin	-122.27	37.80
Cymric (Phacoides/Carneros)	3800	23	San Joaquin Basin	-118.86	35.49
Santa Fe Springs (Main Area)	5400	33	Los Angeles Basin	-118.24	34.05
Dominquez (Pliocene-Miocene)	4000	30	Los Angeles Basin	-118.28	33.83
Brea Olinda (Pliocene-Miocene)	3240	18.4	Los Angeles Basin	-117.85	33.78
Torrance (Main)	3740	19	Los Angeles Basin	-118.24	34.05
Ventura (All)	8750	31	Coastal Districts	-119.29	34.28
San Miguelito (all)	6705	30.5	Coastal Districts	-119.29	34.28

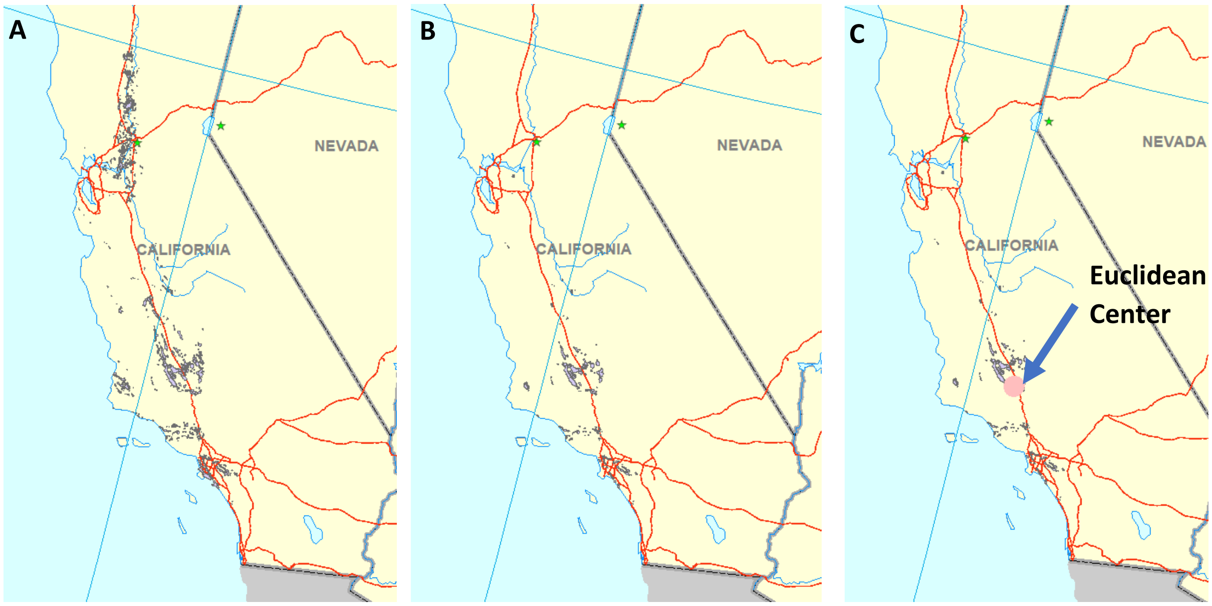

Figure A3. This map shows (A) all the oil and gas wells in California, as well as (B) those specifically relevant for EOR. The Euclidean center of the EOR-specific locations is shown in (C) as a dot and this is considered as the single storage location for network architecture in our analysis.

Macroalgae is not currently used as fuel for biomass power plants in the California basin. For this study, it is assumed that current fossil fuel power plants will be converted to make use of macroalgae-based in the future, as fossil fuels are gradually phased out. It is presumed that A-BECCS power plants will not replace existing renewable power plants in the long-term future, because the latter are generally constructed in specific locations where climatic conditions and/or policy initiatives make it especially appealing to use a particular kind of biomass fuel.

Accordingly, it is assumed that CO_2 source locations correspond to the locations of existing fossil fuel power plants in the California basis. These locations were collected from the WESTCARB GIS Database [81].

As discussed, a cluster radius of 300 miles is assumed as consistent with the 2°C climate targets. Further, representative pipeline networks are drawn to simulate their specifications and obtain high, medium and low environmental burdens per functional unit generated. These architectures depict prospective networks in highly to lowly clustered cases, which is important to consider because of economies-of-scale.

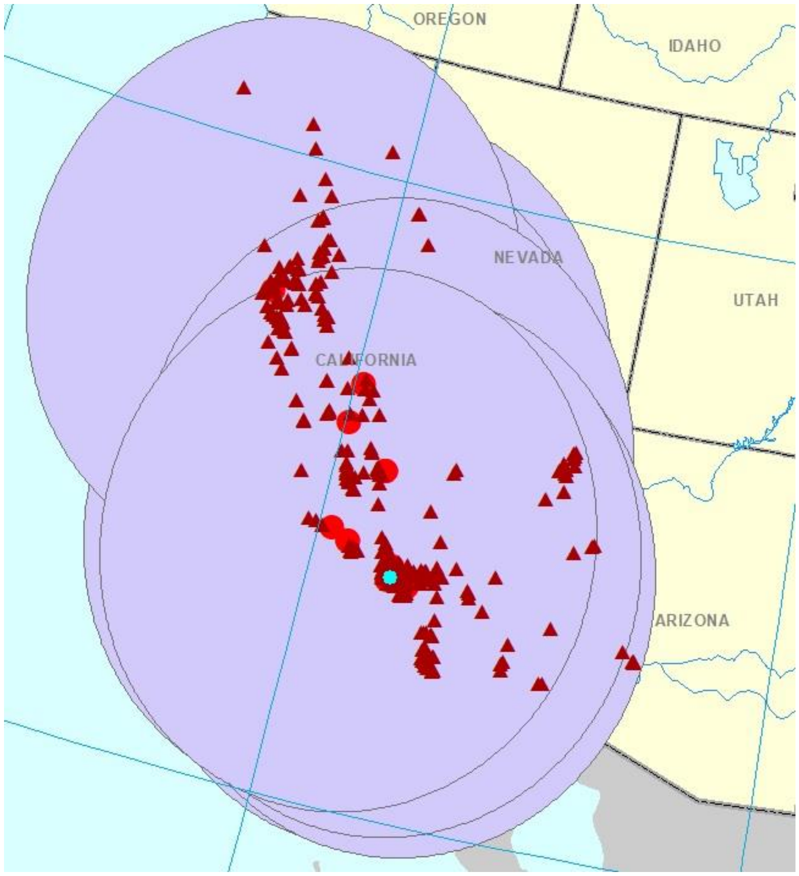

Figure A4. Assumed storage location and prospective source locations around it. The blue circle represents a 300-mile radius around the storage location

The Gulf Coast

For the Gulf Coast, which is associated with the SECARB partnership, CO_2 sequestration has been discussed in detail for the Louisiana, Mississippi and Alabama panhandles. Here, we discuss the potential sinks and adjoining sources as discussed in the literature.

Louisiana has observed a decrease in the number of active wells and stagnation in total oil production over the past three decades. Secondary methods are being employed; however, there is a significant potential for CO_2-EOR in this region with pilots having been carried out in both miscible and immiscible EOR realms. Figure A5 illustrates various oil wells in the state, which may be seen to be spread throughout.

Subsequently, we referred to the ARI report on EOR potential in the gulf coast because of the presence of several distinct oil fields in this region [83]. Accordingly, four reservoirs with high EOR feasibility have been indicated in Table A4. It may be observed that these are at a significantly higher depth than seen for Californian basins. Accordingly, coordinates for the three separate counties are collected by carrying out Google Internet search. Also, EOR feasibility is much higher at the coasts than inland (Figure A5), which bodes well for aquatic biomass infrastructure.

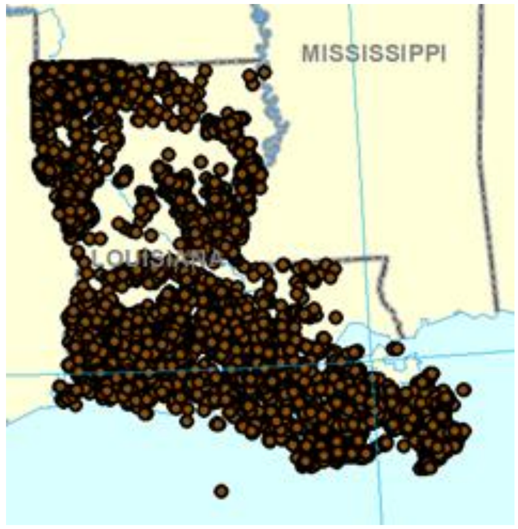

Figure A5. Oil wells in Louisiana, courtesy Louisiana Geographic Information Center and downloaded from [5]

Table A4. Fields suitable for CO_2-EOR in Louisiana from ARI [83]

Name of field	Depth (feet)	Oil Gravity (API)	County
Callilou Island	13,000	39	Terrebonne Parish
Lake Washington	12,500	26	Plaquemines Parish
Weeks Island	14,000	33	Iberia Parish
West Bay	9,000	30	Plaquemines Parish

In addition to these fields, the Delhi field (located near Monroe, LA) is being explored by Denbury as a potential opportunity for EOR.

Significant EOR operations are known to be carried out in Mississippi as well, where initial opportunities for Plant Ratcliffe or the Kemper Project were also explored [148]. Denbury has provided details of several EOR initiatives such as [149]

- Heidelberg Field, located in Jasper County, where injection began in later 2008
- Tinsley field, located in the Yazoo County
- West Yellow Creek field, located in the Wayne County, where CO_2 flood operations are planned

The Tinsley and Heidelberg fields are also considered as a potential EOR option in the ARI survey [83]. Also, other fields have been considered as shown in Table A5. For reference, it may be noted that West Eucutta and West Heidelberg have been considered as potential immiscible-EOR options and contain heavy oil. Accordingly, coordinates for the three separate counties are collected by carrying out Google Internet search.

Table A5. Fields suitable for CO_2-EOR in Louisiana from ARI [83]

NAME OF FIELD	DEPTH (FEET)	OIL GRAVITY (API)	COUNTY
Tinsley	4,900	33	Yazoo
Quitman Bayou	4,700	39	Adams
East Heidelberg	4,827	25	Jasper
West Eucutta	4,900	23	Wayne
West Heidelberg	5,000	22	Jasper

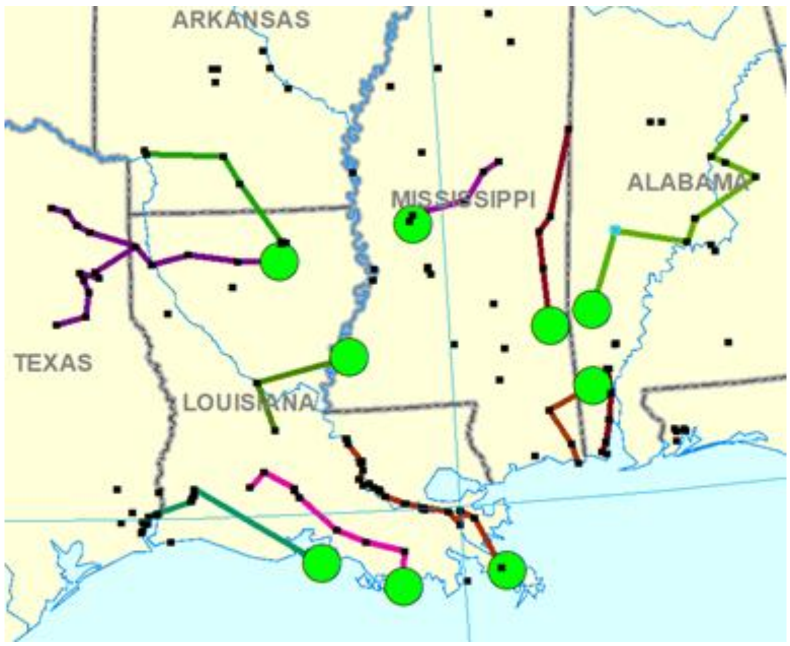

Figure A6. Prospective pipeline architecture in the gulf coast

Alabama oil fields have also been considered as important EOR avenues. For instance, the Citroneile and Womack Hill oilfields have been indicated by ARI and Esposito et al. to be feasible EOR fields with depths of 11,000-12,000 ft and oil gravity ~40 API [83], [150]. These correspond to the southern oilfields in Alabama and accordingly these southern Alabama oilfields have been marked up from the SECARB Phase 1 outcomes [151].

Further, power plant coordinates within 300 miles of these potential sinks were collected from the US EIA database and potential pipeline networks are drawn to estimate embodied environmental damages [19].

Permian Basin

The Permian Basin covering western Texas and New Mexico has impressive prospects for EOR. The ARI report suggests that at the time of preparation of that report, there were 26 oilfields with a total production of more than 166,000 bopd [84]. Further, as pointed out in the same report, there is a localization of the several sites were EOR prospects are seen i.e. within the area near the Texas-New Mexico border, most of the storage opportunities are noticed within an area less than 15,000 sq. miles (Figure A7).

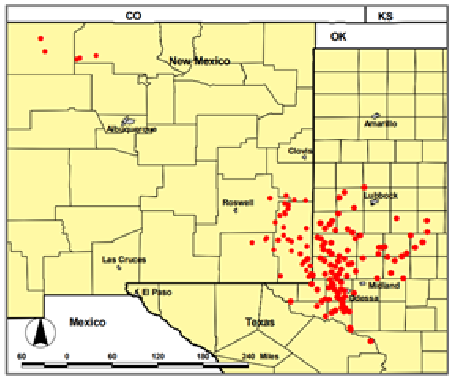

Figure A7. Oil wells in the Permian basin amenable to EOR

As done with other oilfields, we refer to the ARI work for discretizing CO_2 sinks for effective geospatial analysis and constructing pipeline architecture. Because of the localized reservoirs, we consider a single Euclidean center of the entire basin as shown in Figure A8 with data extracted from the UT Austin Bureau of Geosciences webpage [152].

Figure A8. Permian basin outline and calculated Euclidean center (in yellow)

Again, closely located potential CO_2 sources are then marked on the map and prospective pipelines are drawn, which yields the results shown in Figure A9.

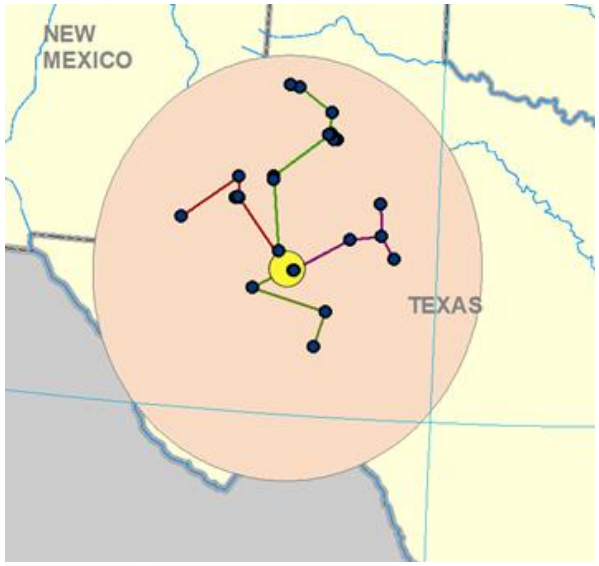

Figure A9. Prospective pipeline architecture in the Gulf Coast

7. CO_2 transport through pipelines

Environmental damages and energy consumption arising from CO_2 transport were evaluated, with accounting for both construction and operation of the pipeline network.

7.1. Pipeline specifications

Principle design parameters include transport distance, volumetric throughput, pressure differential, diameter, and wall thickness.

A pressure differential is required to transport CO_2 via pipeline between source and sink. It is assumed that CO_2 is compressed to a starting pressure of 15.3 MPa at the source location (i.e., the power plant). It is also assumed that the desired pressure at the sequestration site is 8 MPa so that CO_2 exists in a supercritical state; thereby occupying significantly less volume than in the gaseous phase, and facilitating easier management and more efficient sequestration [84].

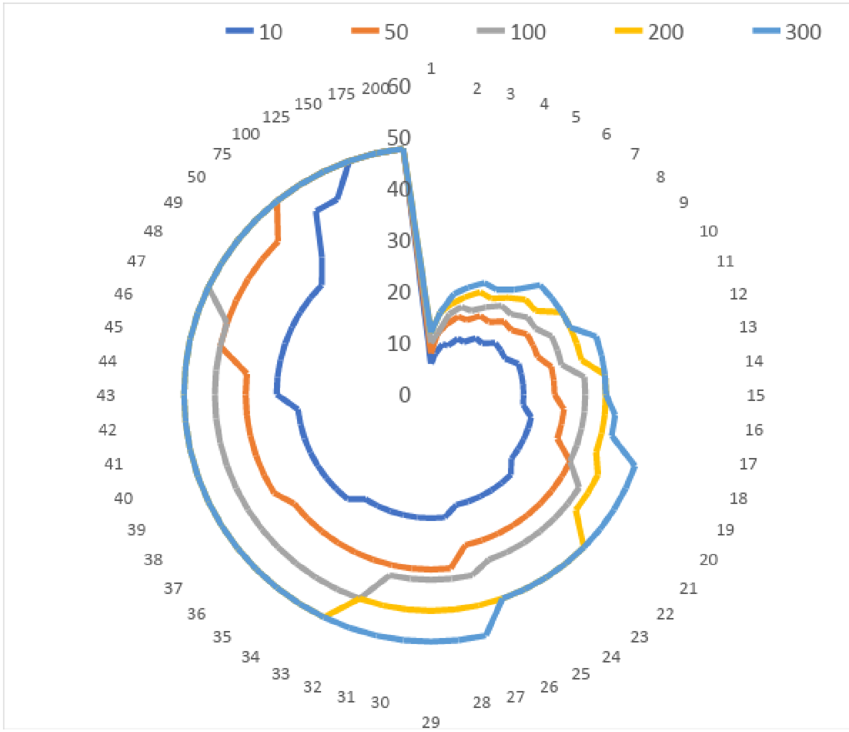

Figure A10. Illustrative radar chart showing the nominal diameter of a CO_2 pipeline, as computed using the IECM framework. Output diameter is computed in inches (discretely, based on the US Code of Federal Regulations), and it is illustrated as a radial distance from the center point. These values are selected based on throughput volume and transport distance. The throughput volume ranges from 0-200 Mt-CO_2/year. It is depicted axially as a circle. Five representative pipeline lengths are illustrated: 10, 50, 100, 200 and 300 km. These are illustrated using five different colored lines.

Taking into account anticipated volumetric throughput and the desired pressure differential, the pipe inner diameter can be computed as a function of several additional parameters, including fluid compressibility, temperature, pressure gradient (as indicated above), average pressure, and CO_2 molecular weight [153]. However, using a non-linear analytical expression to compute this parameter for many combinations of known inputs is highly time-consuming. Also, it is somewhat meaningless to compute pipe diameter across a continuous range, given that pipes are produced by manufacturers in discrete sizes [154]. For this reason, the Integrated Environmental Control Model (IECM) was used to assign a nominal pipe diameter based on the design parameters referenced above. This application was developed at Carnegie Mellon University, and it is available for open-access (https://www.cmu.edu/epp/iecm/). It has been widely used for previous CCS modeling in the United States and internationally [155]–[158]. In this study, IECM was used to produce nominal diameter curves for various combinations of throughput volume and transport distance. The results of the IECM analysis are summarized in Figure A10.

Once the nominal pipe diameter has been assigned, the thickness of the pipe wall is computed using methodology from the US Code of Federal Regulations:

$$Pipeline\ thickness\ (inch) = \frac{p_{mop} D_o}{2SEF} \qquad Eq. A8$$

Where p_{mop} is the maximum operating pressure in the pipeline (15.3 MPa), D_o is the outside pipe diameter obtained from IECM (see Figure A10), S is the minimum yield stress for commercial steel pipe (483 MPa), E is the longitudinal joint factor (1.0), and F is the design factor (0.72). Values of p_{mop}, S, E, and F for this study are set to the default parameters from IECM [159].

7.2. Construction environmental burdens

Pipe diameter and thickness are used to compute the volume (and thus, mass) of steel used for pipeline construction based on geometric formulas, as shown below:

$$Mass\ of\ steel = \rho\pi \times \frac{D_o^2 - D_i^2}{4} \times l = \rho\pi \times \frac{(D_o + D_i)(D_o - D_i)}{4} \times l = \rho\pi \times \frac{(2D_o - t)(t)}{4} \times l \quad Eq. A9$$

Where D_i denotes internal diameter, l denotes pipeline length, and ρ is the density of steel (7,900 kg/m^3)[160]. This mass is then multiplied by energy use and emissions factors from GREET 2018 .Net (Table A6) [72]. These data account for coke production, sintering, operation of a blast furnace and basic oxygen furnace, and on-site generation processes.

Table A6: Life-cycle environmental burdens associated with steel production, from GREET 2018 .Net [161]

Parameter	Unit	Value
CO_2 emission	kg-CO_2/kg-steel	2.02
CH_4 emission	g-CH_4/kg-steel	3.46
Energy consumption	MJ/kg-steel	21

It is anticipated that the installation of the pipeline network will be very economically burdensome (e.g., labor costs are very expensive); however, previous analysis by NREL has revealed that the environmental impacts of pipeline installation are significantly less than the economic impacts [64]. For this reason, installation activities are excluded from this analysis.

7.3. Operational burdens from CO_2 transport

Environmental impacts arise from the operation of the piped network to transport CO_2. These emissions occur throughout the duration that CO_2 is being transported and are directly dependent on the mass of CO_2 transported through the system. McCoy reports booster compression power requirements to be 1.43 kWh/t-CO_2 for compression from 10 MPa to 14 MPa [159]. Accordingly, environmental impacts associated with compression for CO_2 transport are calculated by multiplying this value by regional grid impact factors in Table 1 of the manuscript.

7.4. CO_2 leakage from pipelines

It is anticipated that pipeline leakage of CO_2 will contribute to life-cycle GWP. This is accounted for based on significant measured data from the natural gas industry. Lamb et al. have undertaken extensive surveys of pipeline leaks in natural gas distribution systems, and report leakage rates of 0.10-0.22% [79]. The natural gas distribution network varies by region; however, this is a result of differences in management practices and not necessarily, innate geographical distinctions. In the current study, it is assumed that CO_2 transport pipelines will be newly constructed and will, therefore, exhibit uniform leakage on the order of 0.16% (assuming the national average [79]).

7.5. Emission estimation for CO_2 injection and oil recovery processes

The amount of CO_2 to be injected into the oil reservoirs is taken from the preceding models as a function of several parameters and is equal to the sum of CO_2 emissions from the power plants (as calculated in the preceding subsection inform the final throughput of each pipeline network) and the CO_2 stream from the PSA system installed in the anaerobic digestor unit.

Several sources in the literature have accounted for the effectiveness of the EOR system i.e. the amount of CO_2 required to extract a unit incremental amount of oil. For instance, Heddle et al. (2003) have used the CO_2 effectiveness of 85-227 scm/bbl while Abotalib et al. have derived their values from NETL (2014) which is variant on the basin [18], [162]. We have used the injection-production profiles from the ARI reports for the three basins and consider the cumulative amounts of CO_2-oil ratios in the life-cycle since oil production declines in the latter half of the well (considering a conventional oilfield). Further, some amount of energy is also expended on treating the high saline oil & gas brine produced from these oilfields. Again, we use the cumulative water-oil ratio from these oilfields as detailed in the ARI reports, as shown in Table A7.

Another important methodological point is that a significant amount of CO_2 after injection is again produced as the lifetime of the oilfield advances. The produced CO_2 is again reinjected in the latter years. Thus, the purchased CO_2 i.e. fresh stream of CO_2 derived from a Large Point Source (LPS) and the gross amount of CO_2 injected are different, as indicated below [163]:

$$\frac{Purchased\ CO_2}{Injected\ CO_2} = \%Retention$$

Similarly, some of the water produced earlier on is later injected for flooding the reservoir which is the secondary oil recovery method.

Several open-source life-cycle models have been utilized off-late to model life-cycle implications of oil & gas systems. For instance, Cooney et al. (2014) utilized OPGEE (Oil Production Greenhouse gas Emissions Estimator), Petroleum Refinery Life Cycle Inventory Model (PRELIM) and GreenHouse gas emissions of current Oil Sands Technologies (GHOST) tools to estimate life-cycle implications of American petroleum GHG emissions in various stages [164].

In this paper, we use the OPGEE framework (version 3.0) for our purposes. This is the most recent version of the OPGEE tool framework and allows for life-cycle analyses for CO_2-EOR. One of the initial papers on OPGEE has focused on calibrating it to respond it to the properties of the oil and the oilfield [89]. Foremost amongst these are oil gravity and depth. Also important for simulating the net GHG/energy implications are total oil production, gas-oil ratio, and water-oil ratio – all of which can be estimated or read from the basin level production-injection profiles shown in Table A7. Accordingly, we model the fields in the OPGEE framework, distributions of the results are shown in Table A7. Once the corresponding model runs are carried out in OPGEE, the GWP and of the EOR stage are calculated as shown in Table A7. Summary of parameters for both CO_2 pipeline and storage are in Table A8.

Table A7. Production injection profiles for the three oil basins studied as simulated by ARI

Basin	Time simulated (years)	Oil produced (Mbbl)	CO2 injected (MMcf)	CO2 purchased (MMcf)	Water injected (Mbw)	Water produced (Mbw)
California	23	978	13,431	10,022	5,505	6,354
Gulf Coast	23	978	15,590	5,327	5,909	6,685
Permian	23	12,391	159,009	55,842	46,539	55,713

Table A8. Parameter summary for CO_2 pipeline and storage

Input	Units	Min	Likely (Median)	Max	Distribution	Source
CO_2 Pipeline Parameters						
Mass of steel for total throughput of CO_2	kg steel/kg CO_2	2.94E-03	6.19E-03	9.54E-03	Uniform	[87], [153]
Steel embodied CO_2 emissions	$kgCO_2$/kg steel	-	2.02	-	-	[72]
Steel embodied CH_4 emissions	gCH_4/kg steel	-	3.46	-	-	[72]
Fugitive emissions (produced biogas)	%	-	0.10	-	-	[73]
CO_2 compressions energy use	kWh/tCO_2	-	6.5	-	-	[159]
CO_2 Storage Parameters						
Energy consumption for EOR	MJ_{out}/ $MJ_{produced}$	0.27	0.29	0.31	Triangular	[78], [79]
CO_2 emission factor for EOR	gCO_2/MJ crude	12.51	13.05	13.35	Triangular	[80]
CO_2 injection: oil production	tCO_2/bbl crude	0.41 1.00 0.40	0.45 (EC) 1.13 (GM) 0.40 (WC)	0.45 1.13 0.40	Triangular	[82]–[84]
CO_2 leakage (produced biogas)	%	-	0.09	-	-	[93]
CO_2 from oil combustion	gCO_2/MJ crude	-	70.5	-	-	[165]

8. Sensitivity Analysis

Tornado plots showing the absolute sensitivity of the model by varying one input parameter at a time and its effects on the outputs. The most influential parameters for EROI are: water content, BMP, gVS/kgTS, and energy consumption rate for EOR and is consistent for all clusters. While most influential parameters for GWP are: water content, CO_2 effectiveness for EOR, and carbon content and is consistent for all clusters. The plots shown are for the Gulf of Mexico, Figure A11. In Figure A12 the influential parameters for the Gulf of Mexico without EOR are shown.

Figure A11. Tornado plots for the top 6 influential parameters for the Gulf of Mexico cluster

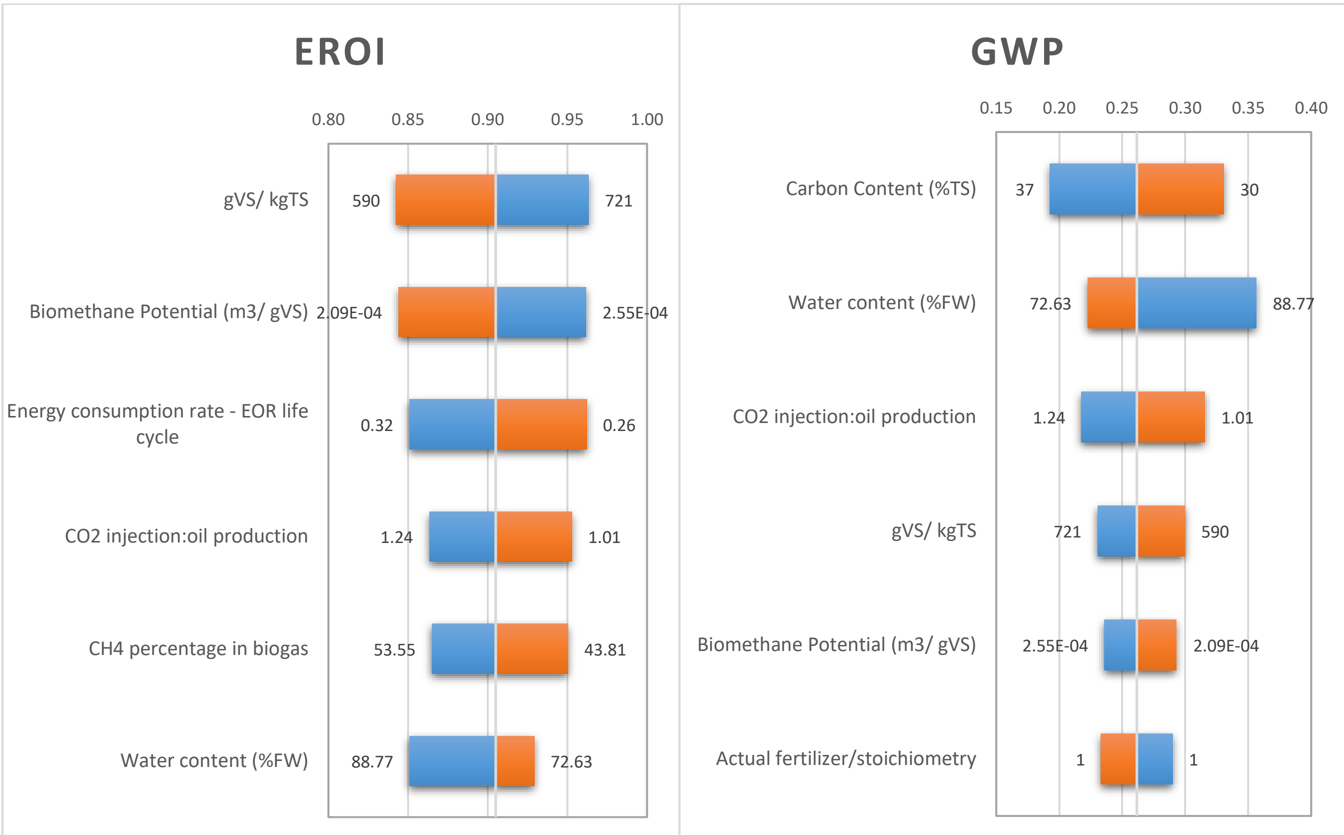

Figure A12. Tornado plots for the top 6 influential parameters for the Gulf of Mexico cluster with no EOR

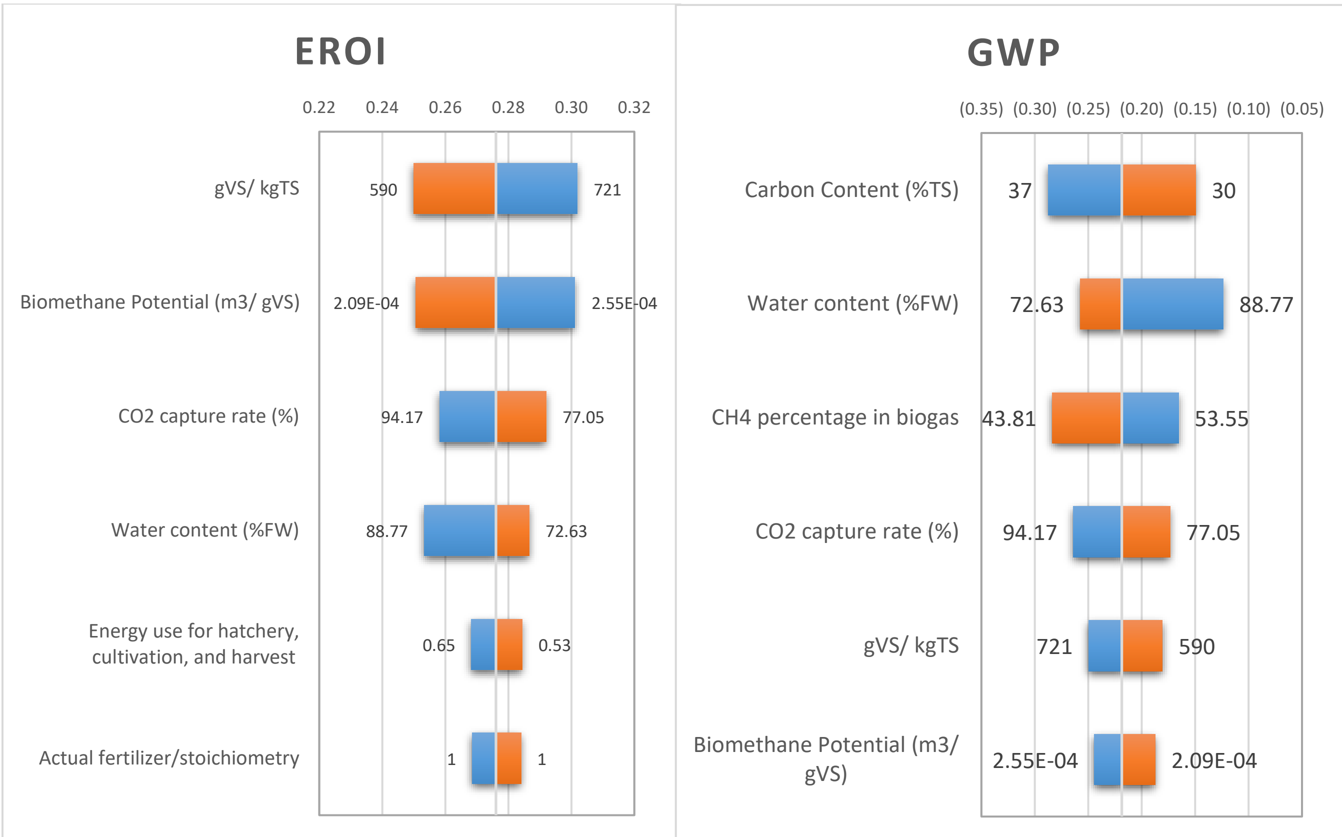

References

[1] D. P. van Vuuren, S. Deetman, J. van Vliet, M. van den Berg, B. J. van Ruijven, and B. Koelbl, “The role of negative CO2 emissions for reaching 2 °C—insights from integrated assessment modelling,” *Clim. Change*, vol. 118, no. 1, pp. 15–27, May 2013, doi: 10.1007/s10584-012-0680-5.

[2] P. Smith *et al.*, “Biophysical and economic limits to negative CO2 emissions,” *Nat. Clim. Change*, vol. 6, no. 1, pp. 42–50, Jan. 2016, doi: 10.1038/nclimate2870.

[3] F. Albanito *et al.*, “Carbon implications of converting cropland to bioenergy crops or forest for climate mitigation: a global assessment,” *Glob. Change Biol. Bioenergy*, vol. 8, pp. 81–95, Dec. 2014.

[4] J. Kemper, “Biomass and carbon dioxide capture and storage: A review,” *Int. J. Greenh. Gas Control*, vol. 40, pp. 401–430, Sep. 2015, doi: 10.1016/j.ijggc.2015.06.012.

[5] V. Stavrakas, N.-A. Spyridaki, and A. Flamos, “Striving towards the Deployment of Bio-Energy with Carbon Capture and Storage (BECCS): A Review of Research Priorities and Assessment Needs,” *Sustainability*, vol. 10, no. 7, 2018, doi: 10.3390/su10072206.

[6] J. K. Costanza, R. C. Abt, A. J. McKerrow, and J. A. Collazo, “Bioenergy production and forest landscape change in the southeastern United States,” *GCB Bioenergy*, vol. 9, no. 5, pp. 924–939, 2017, doi: 10.1111/gcbb.12386.

[7] C. M. Duarte, J. J. Middelburg, and N. Caraco, “Major role of marine vegetation on the oceanic carbon cycle,” *Biogeosciences*, no. 2, p. 8, 2005.

[8] M. E. Capron, J. R. Stewart, and R. K. Rowe, “Secure seafloor container CO2 storage,” in *2013 OCEANS - San Diego*, Sep. 2013, pp. 1–8, doi: 10.23919/OCEANS.2013.6741182.

[9] A. de R. N‘Yeurt, D. P. Chynoweth, M. E. Capron, J. R. Stewart, and M. A. Hasan, “Negative carbon via Ocean Afforestation,” *Process Saf. Environ. Prot.*, vol. 90, no. 6, pp. 467–474, Nov. 2012, doi: 10.1016/j.psep.2012.10.008.

[10] J. Langlois, J.-F. Sassi, G. Jard, J.-P. Steyer, J.-P. Delgenes, and A. Helias, “Life cycle assessment of biomethane from offshore-cultivated seaweed,” *Biofuels Bioprod. Biorefinery*, vol. 6, no. 4, pp. 387–404, Aug. 2012.

[11] M. Seghetta *et al.*, “Seaweed as innovative feedstock for energy and feed – Evaluating the impacts through a Life Cycle Assessment,” Accessed: Oct. 21, 2019. [Online]. Available: https://www.sciencedirect.com/science/article/pii/S0959652617302263.

[12] A. D. Hughes, K. D. Black, I. Campbell, K. Davidson, M. S. Kelly, and M. S. Stanley, “Does seaweed offer a solution for bioenergy with biological carbon capture and storage,” *Greenh. Gases*, vol. 2, no. 6, pp. 402–407, Dec. 2012.

[13] R. M. Cuéllar-Franca and A. Azapagic, “Carbon capture, storage and utilisation technologies: A critical analysis and comparison of their life cycle environmental impacts,” *J. CO2 Util.*, vol. 9, pp. 82–102, Mar. 2015, doi: 10.1016/j.jcou.2014.12.001.

[14] C. M. Beal, I. Archibald, M. E. Huntley, C. H. Greene, and Z. I. Johnson, “Integrating Algae with Bioenergy Carbon Capture and Storage (ABECCS) Increases Sustainability,” *Earths Future*, vol. 6, no. 3, pp. 524–542, 2018, doi: 10.1002/2017EF000704.

[15] W. A. Ambrose, C. Breton, M. H. Holtz, V. Núñez-López, S. D. Hovorka, and I. J. Duncan, “CO2 source-sink matching in the lower 48 United States, with examples from the Texas Gulf Coast and Permian Basin,” *Environ. Geol.*, vol. 57, no. 7, pp. 1537–1551, Jun. 2008.

[16] G. Roesijadi *et al.*, “Macroalgae Analysis A National GIS-based Analysis of Macroalgae Production Potential Summary Report and Project Plan,” Report, Dec. 2011. doi: 10.2172/1039854.
[17] A. W. Geddie and S. G. Hall, “Development of a suitability assessment model for the cultivation of intertidal macroalgae in the United States,” *Sci. Total Environ.*, vol. 699, p. 134327, Jan. 2020, doi: 10.1016/j.scitotenv.2019.134327.
[18] M. Abotalib, F. Zhao, and A. Clarens, “Deployment of a Geographical Information System Life Cycle Assessment Integrated Framework for Exploring the Opportunities and Challenges of Enhanced Oil Recovery Using Industrial CO2 Supply in the United States,” *ACS Sustain. Chem. Eng.*, vol. 4, no. 9, pp. 4743–4751, Sep. 2016.
[19] US Energy Information Administration, “Electricity data browser - Net generation for all sectors.” https://www.eia.gov/electricity/data/browser/ (accessed Dec. 06, 2019).
[20] Environmental Protection Agency, “The Emissions and Generation Resource Integrated Database,” *Homer Pro 3.3*, 2012. https://www.epa.gov/energy/emissions-generation-resource-integrated-database-egrid (accessed Dec. 06, 2019).
[21] Weather Service, “U.S Climate Data.” https://www.usclimatedata.com/climate/united-states/us (accessed Dec. 06, 2019).
[22] M. Edwards and L. Watson, “Aquaculture explained: Cultivating Laminaria digitata,” 26, 2011.
[23] M. Alvarado-Morales, A. Boldrin, D. B. Karakashev, S. L. Holdt, I. Angelidaki, and T. Astrup, “Life cycle assessment of biofuel production from brown seaweed in Nordic conditions,” *Bioresour. Technol.*, vol. 129, pp. 92–99, Feb. 2013, doi: 10.1016/j.biortech.2012.11.029.
[24] P. D. Kerrison, M. S. Stanley, M. D. Edwards, K. D. Black, and A. D. Hughes, “The cultivation of European kelp for bioenergy: Site and species selection,” *Biomass Bioenergy*, vol. 80, pp. 229–242, Sep. 2015, doi: 10.1016/j.biombioe.2015.04.035.
[25] J. Kim, G. Kraemer, and C. Yarish, “Use of sugar kelp aquaculture in Long Island Sound and the Bronx River Estuary for nutrient extraction,” *Mar. Ecol. Prog. Ser.*, vol. 531, pp. 155–166, Jul. 2015, doi: 10.3354/meps11331.
[26] C. K. Tseng, “Seaweed Resources of North America and Their Utilization,” *Econ. Bot.*, vol. 1, no. 1, pp. 69–97, 1947.
[27] J. J. Milledge and P. J. Harvey, “Golden Tides: Problem or Golden Opportunity? The Valorisation of Sargassum from Beach Inundations,” *J. Mar. Sci. Eng.*, vol. 4, no. 3, p. 60, Sep. 2016, doi: 10.3390/jmse4030060.
[28] M. M. Czyrnek-Delêtre, S. Rocca, A. Agostini, J. Giuntoli, and J. D. Murphy, “Life cycle assessment of seaweed biomethane, generated from seaweed sourced from integrated multi-trophic aquaculture in temperate oceanic climates,” *Appl. Energy*, vol. 196, pp. 34–50, Jun. 2017, doi: https://doi.org/10.1016/j.apenergy.2017.03.129.
[29] G. Wernet, C. Bauer, B. Steubing, J. Reinhard, E. Moreno-Ruiz, and B. Weidema, “The ecoinvent database version 3 (part I): overview and methodology.,” *Int. J. Life Cycle Assess.*, vol. 21, no. 9, pp. 1218–1230.
[30] D. Krause-Jensen, P. Lavery, O. Serrano, N. Marbà, P. Masque, and C. M. Duarte, “Sequestration of macroalgal carbon: the elephant in the Blue Carbon room,” *Biol. Lett.*, vol. 14, no. 6, p. 20180236, Jun. 2018, doi: 10.1098/rsbl.2018.0236.

[31] D. Krause-Jensen and C. M. Duarte, “Substantial role of macroalgae in marine carbon sequestration,” *Nat. Geosci.*, vol. 9, no. 10, pp. 737–742, Oct. 2016, doi: 10.1038/ngeo2790.

[32] V. Vivekanand, “Biogas production from the brown seaweed Saccharina latissima: thermal pretreatment and codigestion with wheat straw,” *J. Appl. Phycol.*, vol. v. 24, no. 5, pp. 1295–1301, Oct. 2012, doi: 10.1007/s10811-011-9779-8.

[33] I. Michalak, “Experimental processing of seaweeds for biofuels,” *Wires Energy Environ.*, vol. 7, no. 3, Jan. 2018, Accessed: Oct. 21, 2019. [Online]. Available: https://onlinelibrary.wiley.com/doi/full/10.1002/wene.288.

[34] F. C. Ertem, P. Neubauer, and S. Junne, “Environmental life cycle assessment of biogas production from marine macroalgal feedstock for the substitution of energy crops,” *J. Clean. Prod.*, vol. 140, pp. 977–985, Jan. 2017.

[35] G. Jard, H. Marfaing, H. Carrère, J. P. Delgenes, J. P. Steyer, and C. Dumas, “French Brittany macroalgae screening: Composition and methane potential for potential alternative sources of energy and products,” *Bioresour. Technol.*, vol. 144, pp. 492–498, Sep. 2013, doi: 10.1016/j.biortech.2013.06.114.

[36] S. Tedesco, D. M. Lochlainn, and A. G. Olabi, “Particle size reduction optimization of Laminaria spp. biomass for enhanced methane production - ScienceDirect,” *Energy*, vol. 76, pp. 857–862, Nov. 2014.

[37] Y. N. Barbot, H. Al-Ghaili, and R. Benz, “A Review on the Valorization of Macroalgal Wastes for Biomethane Production,” *Mar. Drugs*, vol. 14, no. 6, Jun. 2016, Accessed: Oct. 21, 2019. [Online]. Available: https://www.ncbi.nlm.nih.gov/pmc/articles/PMC4926079/.

[38] S. Tedesco, K. Y. Benyounis, and A. G. Olabi, “Mechanical pretreatment effects on macroalgae-derived biogas production in co-digestion with sludge in Ireland,” *Energy*, vol. 61, pp. 27–33, Nov. 2013, doi: 10.1016/j.energy.2013.01.071.

[39] D. Manns, A. L. Deutschle, B. Saake, and A. S. Meyer, “Methodology for quantitative determination of the carbohydrate composition of brown seaweeds (Laminariaceae),” *RSC Adv.*, vol. 4, no. 49, pp. 25736–25746, Jun. 2014, doi: 10.1039/C4RA03537B.

[40] M. M. Nielsen *et al.*, “Variation in biochemical composition of Saccharina latissima and Laminaria digitata along an estuarine salinity gradient in inner Danish waters,” *Algal Res.*, vol. 13, pp. 235–245, Jan. 2016, doi: 10.1016/j.algal.2015.12.003.

[41] C. Herrmann, J. FitzGerald, R. O’Shea, A. Xia, P. O’Kiely, and J. D. Murphy, “Ensiling of seaweed for a seaweed biofuel industry,” *Bioresour. Technol.*, vol. 196, pp. 301–313, Nov. 2015, doi: 10.1016/j.biortech.2015.07.098.

[42] M. Soto, M. A. Vázquez, A. de Vega, J. M. Vilariño, G. Fernández, and M. E. S. de Vicente, “Methane potential and anaerobic treatment feasibility of Sargassum muticum,” *Bioresour. Technol.*, vol. 189, pp. 53–61, 2015, doi: 10.1016/j.biortech.2015.03.074.

[43] D. P. Chynoweth, D. L. Klass, and sambhunath Ghosh, “Biomethanation of Giant Brown Kelp Macrocystis Pyrifera,” *Energy Biomass Wastes*, 1978.

[44] K. Anjaneyulu, S. J. Tarwadi, and D. J. Mehta, “Anaerobic digestion of seaweed for biogas: A kinetic evaluation,” *Chem. Technol. Biotechnol.*, vol. 45, no. 1, pp. 5–14, 1989.

[45] A. D. Sutherland and J. C. Varela, “Comparison of various microbial inocula for the efficient anaerobic digestion of Laminaria hyperborea,” *BMC Biotechnol.*, vol. 14, no. 1, p. 7, Dec. 2014, doi: 10.1186/1472-6750-14-7.

[46] C. H. Vanegas and J. Bartlett, “Green energy from marine algae: biogas production and composition from the anaerobic digestion of Irish seaweed species,” *Environ. Technol.*, vol. 34, no. 15, pp. 2277–2283, Feb. 2013.
[47] I. Angelidaki, D. Karakashev, and M. Alvarado-Morales, “Anaerobic Co-digestion of Cast Seaweed and Organic Residues,” 2013.
[48] S. Sharma, L. Neves, J. Funderud, L. T. Mydland, M. Øverland, and S. J. Horn, “Seasonal and depth variations in the chemical composition of cultivated Saccharina latissima,” *Algal Res.*, vol. 32, pp. 107–112, Jun. 2018, doi: 10.1016/j.algal.2018.03.012.
[49] J. A. Gallagher, L. B. Turner, J. M. M. Adams, S. Barrento, P. W. Dyer, and M. K. Theodorou, “Species variation in the effects of dewatering treatment on macroalgae,” *J. Appl. Phycol.*, vol. 30, no. 4, pp. 2305–2316, Aug. 2018, doi: 10.1007/s10811-018-1420-7.
[50] J. A. Gallagher, L. B. Turner, J. M. M. Adams, P. W. Dyer, and M. K. Theodorou, “Dewatering treatments to increase dry matter content of the brown seaweed, kelp (Laminaria digitata,” *Bioresour. Technol.*, vol. 224, pp. 662–669, Jan. 2017, doi: 10.1016/j.biortech.2016.11.091.
[51] “Engineering ToolBox,” *Methane - Density and Specific Weight*, 2018. https://www.engineeringtoolbox.com/methane-density-specific-weight-temperature-pressure-d_2020.html (accessed Jan. 19, 2020).
[52] “Engineering ToolBox,” *Fuels - Higher and Lower Calorific Values*, 2013. https://www.engineeringtoolbox.com/fuels-higher-calorific-values-d_169.html (accessed Jan. 19, 2020).
[53] O. Eriksson, *Environmental Technology Assessment of Natural Gas Compared to Biogas*. InTech: Primoz Potocnik (Ed.), 2010.
[54] S. Tedesco and J. Stokes, “Valorisation to biogas of macroalgal waste streams: a circular approach to bioproducts and bioenergy in Ireland,” *Chem. Zvesti*, vol. 71, no. 4, pp. 721–728, 2017, doi: 10.1007/s11696-016-0005-7.
[55] M. Edward, S. Edwards, U. Egwu, and P. Sallis, “Bio-methane potential test (BMP) using inert gas sampling bags with macroalgae feedstock,” *Biomass Bioenergy*, vol. 83, pp. 516–524, Dec. 2015, doi: 10.1016/j.biombioe.2015.10.026.
[56] M. E. Montingelli, K. Y. Benyounis, B. Quilty, J. Stokes, and A. G. Olabi, “Optimisation of biogas production from the macroalgae Laminaria sp. at different periods of harvesting in Ireland,” *Appl. Energy*, vol. 177, pp. 671–682, Sep. 2016, doi: 10.1016/j.apenergy.2016.05.150.
[57] M. R. Tabassum, D. M. Wall, and J. D. Murphy, “Biogas production generated through continuous digestion of natural and cultivated seaweeds with dairy slurry,” *Bioresour. Technol.*, vol. 219, pp. 228–238, Nov. 2016, doi: 10.1016/j.biortech.2016.07.127.
[58] M. D’Este, M. Alvarado-Morales, A. Ciofalo, and I. Angelidaki, “Macroalgae Laminaria digitata and Saccharina latissima as Potential Biomasses for Biogas and Total Phenolics Production: Focusing on Seasonal and Spatial Variations of the Algae,” *Energy Fuels*, vol. 31, no. 7, pp. 7166–7175, Jul. 2017, doi: 10.1021/acs.energyfuels.7b00853.
[59] J. J. Milledge, B. V. Nielsen, M. S. Sadek, and P. J. Harvey, “Effect of Freshwater Washing Pretreatment on Sargassum muticum as a Feedstock for Biogas Production,” *Energies*, vol. 11, no. 7, p. 1771, Jul. 2018, doi: 10.3390/en11071771.

[60] D. P. Chynoweth, “Review of Biomethane from Marine Biomass,” *Mar. Agron.*, 2002, Accessed: Sep. 24, 2019. [Online]. Available: http://marineagronomy.org/node/118.

[61] S. Ghosh, D. L. Klass, and D. P. Chynoweth, “Bioconversion of Macrocystis pyrifera to methane,” *J. Chem. Technol. Biotechnol.*, vol. 31, no. 1, pp. 791–807, 1981, doi: 10.1002/jctb.5033101105.

[62] M. Song, H. D. Pham, J. Seon, and H. C. Woo, “Overview of anaerobic digestion process for biofuels production from marine macroalgae: A developmental perspective on brown algae,” *Korean J. Chem. Eng.*, vol. 32, no. 4, pp. 567–575, Apr. 2015, doi: 10.1007/s11814-015-0039-5.

[63] “Power blocks in natural gas-fired combined-cycle plants are getting bigger - Today in Energy - U.S. Energy Information Administration (EIA).” https://www.eia.gov/todayinenergy/detail.php?id=38312 (accessed Jan. 22, 2020).

[64] P. L. Spath and M. K. Mann, “Life Cycle Assessment of a Natural Gas Combined Cycle Power Generation System,” NREL/TP-570-27715, 776930, Dec. 2000. doi: 10.2172/776930.

[65] S. Soda, Y. Iwai, K. Sei, Y. Shimod, and M. Ike, “Model analysis of energy consumption and greenhouse gas emissions of sewage sludge treatment systems with different processes and scales,” *Water Sci. Technol.*, vol. 61, no. 2, pp. 365–373, Jan. 2010, doi: 10.2166/wst.2010.827.

[66] B. Puchajda and J. Oleszkiewicz, “Impact of sludge thickening on energy recovery from anaerobic digestion,” *Water Sci. Technol. J. Int. Assoc. Water Pollut. Res.*, vol. 57, no. 3, pp. 395–401, 2008, doi: 10.2166/wst.2008.021.

[67] M. Terhan and K. Comakli, “Energy and exergy analyses of natural gas-fired boilers in a district heating system,” *Appl. Therm. Eng.*, vol. 121, pp. 380–387, Jul. 2017, doi: 10.1016/j.applthermaleng.2017.04.091.

[68] “Natural gas conversion guide,” International Gas Union, 2012.

[69] N. Voća, T. Krička, T. Ćosić, V. Rupić, Ž. Jukić, and S. Kalambura, “Digested residue as a fertilizer after the mesophilic process of anaerobic digestion,” *Plant Soil Environ.*, vol. 51, no. No. 6, pp. 262–266, Nov. 2011, doi: 10.17221/3584-PSE.

[70] A. Petersson and A. Wellinger, “Biogas upgrading technologies – developments and innovations,” IEA, Oct. 2009. [Online]. Available: https://www.ieabioenergy.com/publications/biogas-upgrading-technologies-developments-and-innovations/.

[71] Aspen Environmental Group, “Update to Gas Storage Needed to Support Electricity Generation,” 2012. [Online]. Available: https://www.energy.gov/sites/prod/files/2015/04/f21/AttachB_Aspen_GasStorage2012.pdf.

[72] Argonne National Lab, “Argonne GREET Model,” 2016. https://greet.es.anl.gov/ (accessed Nov. 06, 2019).

[73] “Renewable Energy and CHP | Guides | Carbon Trust.” https://www.carbontrust.com/resources/guides/renewable-energy-technologies/renewable-energy-and-combined-heat-and-power-chp/ (accessed Nov. 06, 2019).

[74] A. B. Rao and E. S. Rubin, “Identifying Cost-Effective CO2 Control Levels for Amine-Based CO2 Capture Systems,” *Ind. Eng. Chem. Res.*, vol. 45, no. 8, pp. 2421–2429, Apr. 2006, doi: 10.1021/ie050603p.

[75] IEA Energy Technology Systems Analysis Programme, “Combined Heat and Power,” May 2010.

[76] L. Angeles, J. Møller, A. Boldrin, and T. H. Christensen, “Anaerobic digestion and digestate use: accounting of greenhouse gases and global warming contribution,” 2009, doi: 10.1177/0734242X09344876.

[77] T. N. Lavoie *et al.*, “Assessing the Methane Emissions from Natural Gas-Fired Power Plants and Oil Refineries,” *Env. Sci Technol*, vol. 51, p. 11, 2017, doi: 10.1021/acs.est.6b05531.

[78] A. Petersson and A. Wellinger, “Biogas upgrading technologies-developments and innovations Task 37-Energy from biogas and landfill gas.”

[79] B. K. Lamb *et al.*, “Direct Measurements Show Decreasing Methane Emissions from Natural Gas Local Distribution Systems in the United States,” *Environ. Sci. Technol.*, vol. 49, no. 8, pp. 5161–5169, Apr. 2015, doi: 10.1021/es505116p.

[80] Wang M, Wu Y, and Elgowainy A, “Argonne GREET Publication : Operating Manual for GREET: Version 1.7,” 2005.

[81] UC Berkley, “WESTCARB GIS data download,” 2018. http://gif.berkeley.edu/westcarb/gis-data/ (accessed Jan. 22, 2020).

[82] Advanced Resources International, Inc., “Basin Oriented Strategies for CO2 Enhanced Oil Recovery: Onshore California Oil Basins,” Department of Energy, Department of Energy, Mar. 2005.

[83] Advanced Resources International, Inc., “Basin Oriented Strategies for CO2 Enhanced Oil Recovery: Gulf Coast,” Department of Energy, Feb. 2006.

[84] Advanced Resources International, Inc., “Basin Oriented Strategies for CO2 Enhanced Oil Recovery: Permian Basin,” Department of Energy, Feb. 2006.

[85] S. Solomon, M. Carpenter, and T. A. Flach, “Intermediate storage of carbon dioxide in geological formations: A technical perspective,” *Int. J. Greenh. Gas Control*, vol. 2, no. 4, pp. 502–510, Oct. 2008, doi: 10.1016/j.ijggc.2008.04.004.

[86] S. T. McCoy and E. S. Rubin, “An engineering-economic model of pipeline transport of CO2 with application to carbon capture and storage,” *Int. J. Greenh. Gas Control*, vol. 2, no. 2, pp. 219–229, Apr. 2008, doi: 10.1016/S1750-5836(07)00119-3.

[87] Carnegie Mellon University, “Integrated Environmental Control Model (IECM) Version 11.2,” 2018. https://www.cmu.edu/epp/iecm/ (accessed Jan. 22, 2020).

[88] M. Mohitpour, H. Golshan, and M. A. Murray, *Pipeline design & construction : a practical approach*, Third edition. New York, New York : ASME Press, 2007.

[89] H. M. El-Houjeiri, A. R. Brandt, and J. E. Duffy, “Open-source LCA tool for estimating greenhouse gas emissions from crude oil production using field characteristics,” *Environ. Sci. Technol.*, vol. 47, no. 11, pp. 5998–6006, Jun. 2013, doi: 10.1021/es304570m.

[90] P. Jaramillo, W. M. Griffin, and S. T. McCoy, “Life Cycle Inventory of CO2 in an Enhanced Oil Recovery System,” *Environ. Sci. Technol.*, vol. 43, no. 21, pp. 8027–8032, Nov. 2009, doi: 10.1021/es902006h.

[91] G. Cooney, J. Littlefield, J. Marriott, and T. J. Skone, "Evaluating the Climate Benefits of CO2-Enhanced Oil Recovery Using Life Cycle Analysis," *Environ. Sci. Technol.*, vol. 49, no. 12, pp. 7491–7500, Jun. 2015, doi: 10.1021/acs.est.5b00700.

[92] C. Wildbolz, "Life Cycle Assessment of Selected Technologies for CO2 Transport and Sequestration," Swiss Federal Institute of Technology Zurich, 2007.

[93] J. Alcalde *et al.*, "Estimating geological CO 2 storage security to deliver on climate mitigation," *Nat. Commun.*, vol. 9, no. 1, pp. 1–13, Jun. 2018, doi: 10.1038/s41467-018-04423-1.

[94] L. Meyer, S. Brinkman, L. van Kesteren, N. Leprince-Ringuet, and F. van Boxmeer, "IPCC Climate Change 2014: Synthesis Report. Contribution of Working Groups I, II and III to the Fifth Assessment Report of the Intergovernmental Panel on Climate Change," p. 169.

[95] S. Manfredi and T. H. Christensen, "Environmental assessment of solid waste landfilling technologies by means of LCA-modeling," *Waste Manag.*, vol. 29, no. 1, pp. 32–43, Jan. 2009, doi: 10.1016/j.wasman.2008.02.021.

[96] F. Xu, Y. Li, X. Ge, L. Yang, and Y. Li, "Anaerobic digestion of food waste – Challenges and opportunities," *Bioresour. Technol.*, vol. 247, pp. 1047–1058, Jan. 2018, doi: 10.1016/j.biortech.2017.09.020.

[97] G. Realmonte *et al.*, "An inter-model assessment of the role of direct air capture in deep mitigation pathways," *Nat. Commun.*, vol. 10, no. 1, p. 3277, Dec. 2019, doi: 10.1038/s41467-019-10842-5.

[98] M. Fajardy and N. M. Dowell, "Can BECCS deliver sustainable and resource efficient negative emissions?," *Energy Environ. Sci.*, vol. 10, no. 6, pp. 1389–1426, Jun. 2017, doi: 10.1039/C7EE00465F.

[99] S. E. Taelman, J. Champenois, M. D. Edwards, S. De Meester, and J. Dewulf, "Comparative environmental life cycle assessment of two seaweed cultivation systems in North West Europe with a focus on quantifying sea surface occupation," *Algal Res.*, vol. 11, pp. 173–183, Sep. 2015, doi: 10.1016/j.algal.2015.06.018.

[100] National Energy Technology Lab, "Best Practices for: Geologic Storage Formation Classification: Understanding Its Importance and Impacts on CCS Opportunities in the United States," Sep. 2010.

[101] A. Gambhir, I. Butnar, P.-H. Li, P. Smith, and S. Neil, "A Review of Criticisms of Integrated Assessment Models and Proposed Approaches to Address These, through the Lens of BECCS," *Energies*, vol. 12, no. 9, May 2019, Accessed: Mar. 29, 2020. [Online]. Available: https://www.mdpi.com/1996-1073/12/9/1747.

[102] R. K. P. and L. A. M. (eds. Contribution of Working Groups I, II and III to the Fifth Assessment Report of the Intergovernmental Panel on Climate Change [Core Writing Team, "IPCC, 2014: Climate Change 2014: Synthesis Report," Gian-Kasper Plattner, 2014.

[103] M. Edwards, L. Watson, F. O'mahony, I. Connellan, P. M. Dring, and A. Werner, "Aquaculture Explained Cultivating Laminaria digitata," 2011.

[104] K. Flavin, N. Flavin, and B. Flahive, "Kelp Farming Manual A Guide to the Processes, Techniques, and Equipment for Farming Kelp in New England Waters," 2013.

[105] C. Rolin, R. Inkster, J. Laing, J. Hedges, and L. Mcevoy, "Seaweed Cultivation Manual Shetland Seaweed Growers Project," 2016.

[106] S. Redmond, L. Green, C. Yarish, J. Kim, and C. Neefus, "New England Seaweed Culture Handbook Nursery Systems," 2014.

[107] Y. Springer, C. Hays, M. Carr, M. Mackey, and J. Bloeser, "Ecology and management of the BULL KELP, NEREOCYSTIS LUETKEANA: A Synthesis with Recommendations for Future Research," 2007.

[108] M. M. Czyrnek-Delêtre, S. Rocca, A. Agostini, J. Giuntoli, and J. D. Murphy, "Life cycle assessment of seaweed biomethane, generated from seaweed sourced from integrated multi-trophic aquaculture in temperate oceanic climates," *Appl. Energy*, vol. 196, pp. 34–50, Jun. 2017, doi: 10.1016/J.APENERGY.2017.03.129.

[109] S. E. Taelman, J. Champenois, M. D. Edwards, S. De Meester, and J. Dewulf, "Comparative environmental life cycle assessment of two seaweed cultivation systems in North West Europe with a focus on quantifying sea surface occupation," *Algal Res.*, vol. 11, pp. 173–183, Sep. 2015, doi: 10.1016/J.ALGAL.2015.06.018.

[110] J. J. Milledge and P. J. Harvey, "Potential process 'hurdles' in the use of macroalgae as feedstock for biofuel production in the British Isles," *J. Chem. Technol. Biotechnol.*, vol. 91, no. 8, pp. 2221–2234, Aug. 2016, doi: 10.1002/jctb.5003.

[111] Fao, "The global status of seaweed production, trade and utilization Volume 124," 2018.

[112] A. H. Buschmann *et al.*, "Seaweed production: overview of the global state of exploitation, farming and emerging research activity," *Eur. J. Phycol.*, vol. 52, no. 4, pp. 391–406, 2017, doi: 10.1080/09670262.2017.1365175.

[113] G. Roesijadi *et al.*, "Macroalgae Analysis A National GIS-based Analysis of Macroalgae Production Potential Summary Report and Project Plan," 2011.

[114] M. Alvarado-Morales, A. Boldrin, D. B. Karakashev, S. L. Holdt, I. Angelidaki, and T. Astrup, "Life cycle assessment of biofuel production from brown seaweed in Nordic conditions," *Bioresour. Technol.*, vol. 129, pp. 92–99, Feb. 2013, doi: 10.1016/J.BIORTECH.2012.11.029.

[115] T. Wernberg, M. S. Thomsen, P. A. Stæhr, and M. F. Pedersen, "Comparative Phenology of Sargassum muticum and Halidrys siliquosa (Phaeophyceae: Fucales) in Limfjorden, Denmark," *Bot. Mar.*, vol. 44, no. 1, Jan. 2001, doi: 10.1515/BOT.2001.005.

[116] A. B. Ross, J. M. Jones, M. L. Kubacki, and T. Bridgeman, "Classification of macroalgae as fuel and its thermochemical behaviour," *Bioresour. Technol.*, vol. 99, no. 14, pp. 6494–6504, Sep. 2008, doi: 10.1016/j.biortech.2007.11.036.

[117] C. M. Moore *et al.*, "Processes and patterns of oceanic nutrient limitation," *Nat. Geosci.*, vol. 6, no. 9, pp. 701–710, Sep. 2013, doi: 10.1038/ngeo1765.

[118] I. Ladner, I. Su, S. Wolfe, and S. Oliver, "Economic Feasibility of Seaweed Aquaculture in Southern California," May 2018.

[119] G. Wernet, C. Bauer, B. Steubing, J. Reinhard, E. Moreno-Ruiz, and B. Weidema, "The ecoinvent database version 3 (part I): overview and methodology," *Int. J. Life Cycle Assess.*, vol. 21, no. 9, pp. 1218–1230, Sep. 2016, doi: 10.1007/s11367-016-1087-8.

[120] EREF, "Internal Research Program Data-driven analysis to guide sustainable solid waste management Anaerobic Digestion of Municipal Solid Waste Report on the State of Practice," 2015.

[121] Y. N. Barbot, L. Thomsen, and R. Benz, "Thermo-Acidic Pretreatment of Beach Macroalgae from Rügen to Optimize Biomethane Production--Double Benefit with

Simultaneous Bioenergy Production and Improvement of Local Beach and Waste Management.," *Mar. Drugs*, vol. 13, no. 9, pp. 5681–705, Sep. 2015, doi: 10.3390/md13095681.

[122] J. Milledge *et al.*, "Effect of Freshwater Washing Pretreatment on Sargassum muticum as a Feedstock for Biogas Production," *Energies*, vol. 11, no. 7, p. 1771, Jul. 2018, doi: 10.3390/en11071771.

[123] C. Herrmann, J. FitzGerald, R. O'Shea, A. Xia, P. O'Kiely, and J. D. Murphy, "Ensiling of seaweed for a seaweed biofuel industry," *Bioresour. Technol.*, vol. 196, pp. 301–313, Nov. 2015, doi: 10.1016/J.BIORTECH.2015.07.098.

[124] J. A. Gallagher, L. B. Turner, J. M. M. Adams, P. W. Dyer, and M. K. Theodorou, "Dewatering treatments to increase dry matter content of the brown seaweed, kelp (Laminaria digitata ((Hudson) JV Lamouroux))," *Bioresour. Technol.*, vol. 224, pp. 662–669, Jan. 2017, doi: 10.1016/J.BIORTECH.2016.11.091.

[125] M. Seghetta *et al.*, "Seaweed as innovative feedstock for energy and feed – Evaluating the impacts through a Life Cycle Assessment," *J. Clean. Prod.*, vol. 150, pp. 1–15, May 2017, doi: 10.1016/J.JCLEPRO.2017.02.022.

[126] J. J. Milledge and P. J. Harvey, "Ensilage and anaerobic digestion of Sargassum muticum," *J. Appl. Phycol.*, vol. 28, no. 5, pp. 3021–3030, Oct. 2016, doi: 10.1007/s10811-016-0804-9.

[127] E. Allen, D. M. Wall, C. Herrmann, A. Xia, and J. D. Murphy, "What is the gross energy yield of third generation gaseous biofuel sourced from seaweed?," *Energy*, vol. 81, pp. 352–360, Mar. 2015, doi: 10.1016/J.ENERGY.2014.12.048.

[128] C. Rodriguez, A. Alaswad, J. Mooney, T. Prescott, and A. G. Olabi, "Pre-treatment techniques used for anaerobic digestion of algae," 2015, doi: 10.1016/j.fuproc.2015.06.027.

[129] R. Ganesh Saratale, G. Kumar, R. Banu, A. Xia, S. Periyasamy, and G. Dattatraya Saratale, "A critical review on anaerobic digestion of microalgae and macroalgae and co-digestion of biomass for enhanced methane generation," *Bioresour. Technol.*, vol. 262, pp. 319–332, 2018, doi: 10.1016/j.biortech.2018.03.030.

[130] H. Ge, P. D. Jensen, and D. J. Batstone, "Relative kinetics of anaerobic digestion under thermophilic and mesophilic conditions," *Water Sci. Technol.*, vol. 64, no. 4, pp. 848–853, 2011, doi: 10.2166/wst.2011.571.

[131] S. Soda, Y. Iwai, K. Sei, Y. Shimod, and M. Ike, "Model analysis of energy consumption and greenhouse gas emissions of sewage sludge treatment systems with different processes and scales," *Water Sci. Technol.*, vol. 61, no. 2, pp. 365–373, 2010, doi: 10.2166/wst.2010.827.

[132] G. D. Gebreeyessus and P. Jenicek, "Thermophilic versus Mesophilic Anaerobic Digestion of Sewage Sludge: A Comparative Review.," *Bioeng. Basel Switz.*, vol. 3, no. 2, Jun. 2016, doi: 10.3390/bioengineering3020015.

[133] J. D. Murphy *et al.*, "A perspective on algal biogas A perspective on algal biogas IEA Bioenergy A perspective on algal biogas," 2015.

[134] G. Jard *et al.*, "Batch and semi-continuous anaerobic digestion of Palmaria palmata: Comparison with Saccharina latissima and inhibition studies," *Chem. Eng. J.*, vol. 209, pp. 513–519, 2012, doi: 10.1016/j.cej.2012.08.010.

[135] G. Jard, H. Marfaing, H. Carrère, J. P. Delgenes, J. P. Steyer, and C. Dumas, "French Brittany macroalgae screening: Composition and methane potential for potential alternative sources of energy and products," *Bioresour. Technol.*, vol. 144, pp. 492–498, 2013, doi: 10.1016/j.biortech.2013.06.114.

[136] "Methane - Density and Specific Weight." https://www.engineeringtoolbox.com/methane-density-specific-weight-temperature-pressure-d_2020.html?vA=20&degree=C&pressure=1bar# (accessed Jul. 01, 2019).

[137] V. Vivekanand, V. G. H. Eijsink, and S. J. Horn, "Biogas production from the brown seaweed Saccharina latissima: thermal pretreatment and codigestion with wheat straw," *J. Appl. Phycol.*, vol. 24, no. 5, pp. 1295–1301, Oct. 2012, doi: 10.1007/s10811-011-9779-8.

[138] M. E. Montingelli, K. Y. Benyounis, B. Quilty, J. Stokes, and A. G. Olabi, "Optimisation of biogas production from the macroalgae Laminaria sp. at different periods of harvesting in Ireland," 2016, doi: 10.1016/j.apenergy.2016.05.150.

[139] J. Bartlett, C. H. Vanegas, and J. Bartlett, "Green energy from marine algae: Biogas production and composition from the anaerobic digestion of Irish seaweed species," *Environ. Technol.*, 2013, doi: 10.1080/09593330.2013.765922.

[140] R. Nkoa, "Agricultural benefits and environmental risks of soil fertilization with anaerobic digestates: a review | SpringerLink," *Agron. Sustain. Dev.*, vol. 34, pp. 473–492, 2014.

[141] J. A. Alburquerque *et al.*, "Assessment of the fertiliser potential of digestates from farm and agroindustrial residues," *Biomass Bioenergy*, vol. 40, pp. 181–189, 2012.

[142] N. Aryal and K. Hjuler, "Review of Biogas Upgrading," 2017.

[143] R. J. Mckee, "Energy Audit of a Typical Compressor Station-Where Waste Heat Comes From."

[144] A. Development Bank, "People's Republic of China: Study on Carbon Capture and Storage in Natural Gas-Based Power Plants (Financed by the Carbon Capture and Storage Fund under the Clean Energy Financing Partnership Facility)," 2014.

[145] EPA, "Efficiency Metrics for CHP Systems: Total System and Effective Electric Efficiencies."

[146] F. Gevaert *et al.*, "Carbon and nitrogen content of Laminaria saccharina in the eastern English Channel: biometrics and seasonal variations," *Mar. Biol.*, vol. 81, pp. 727–734, 2001, doi: 10.1017/S0025315401004532.

[147] S. Manfredi and T. H. Christensen, "Environmental assessment of solid waste landfilling technologies by means of LCA-modeling," *Waste Manag.*, vol. 29, no. 1, pp. 32–43, Jan. 2009, doi: 10.1016/J.WASMAN.2008.02.021.

[148] MEI, "Enhanced Oil Recovery an Ideal Opportunity for Mississippi - Mississippi Energy Institute," 2014. http://www.mei.ms/index.php/2014/03/07/enhanced-oil-recovery-huge-opportunity-for-mississippi/ (accessed Feb. 28, 2020).

[149] "Denbury Resources - CO2 EOR Enhanced Oil Recovery Carbon Dioxide." https://www.denbury.com/operations/gulf-coast-region/tertiary-operations/default.aspx (accessed Feb. 28, 2020).

[150] R. A. Esposito, J. C. Pashin, and P. M. Walsh, "Citronelle Dome: A giant opportunity for multizone carbon storage and enhanced oil recovery in the Mississippi Interior Salt Basin of Alabama," *Environ. Geosci.*, vol. 15, no. 2, pp. 53–62, Jun. 2018.

[151] Geological Survey of Alabama, "Southeastern Regional Carbon Sequestration Partnership (SECARB Phase I)," 2005. http://www2.gsa.state.al.us/CO2/SECARB2/secarb2.htm (accessed Feb. 28, 2020).

[152] Bureau of Economic Geology, "Permian Basin GIS Projects and Databases," 2008. http://www.beg.utexas.edu/resprog/permianbasin/integsynthesis.htm (accessed Feb. 28, 2020).

[153] M. Mohitpour, H. Golshan, and A. Murray, *Pipeline Design & Construction: A Practical Approach, Third Edition*. New York: ASME, 2006.

[154] A. Garg, P. Shukla, S. Parihar, U. Singh, and B. Kankal, "Cost-effective architecture of carbon capture and storage (CCS) grid in India," *Int. J. Greenh. Gas Control*, vol. 66, pp. 129–146, 2017.

[155] H. C. Mantripragada, H. Zhai, and E. S. Rubin, "Boundary Dam or Petra Nova – Which is a better model for CCS energy supply?," *Int. J. Greenh. Gas Control*, vol. 82, pp. 59–68, Mar. 2019, doi: 10.1016/j.ijggc.2019.01.004.

[156] N. Sharma and S. S. Mahapatra, "A preliminary analysis of increase in water use with carbon capture and storage for Indian coal-fired power plants," *Environ. Technol. Innov.*, vol. 9, pp. 51–62, 2018.

[157] H. Gerbelova, P. Versteeg, C. Loakimidis, and P. Ferrão, "The effect of retrofitting Portuguese fossil fuel power plants with CCS," *Appl. Energy*, vol. 101, pp. 280–287, Jan. 2013.

[158] D. B. Gingerich and M. S. Mauter, "Retrofitting the Regulated Power Plant: Optimizing Energy Allocation to Electricity Generation, Water Treatment, and Carbon Capture Processes at Coal-Fired Generating Facilities," *ACS Sustain. Chem. Eng.*, vol. 6, pp. 2694–2703, 2018.

[159] S. T. McCoy, "The Economics of CO2 Transport by Pipeline and Storage in Saline Aquifers and Oil Reservoirs," Engineering & Public Policy, Carnegie Mellon University, 2008.

[160] M. J. Knoope, W. Guijt, A. Ramirez, and A. P. C. Faaij, "Improved cost models for optimizing CO2 pipeline configuration for point-to-point pipelines and simple networks," *Int. J. Greenh. Gas Control*, vol. 22, pp. 25–46, Mar. 2014.

[161] Argonne National Lab, "A fresh design for GREET life cycle analysis tool," 2018. https://greet.es.anl.gov/net (accessed Feb. 28, 2020).

[162] G. Heddle, H. Herzog, and M. Klett, "The Economics of CO2 Storage," *Mass. Inst. Technol.*, p. 115, Aug. 2003.

[163] N. A. Azzolina *et al.*, "How green is my oil? A detailed look at greenhouse gas accounting for CO2-enhanced oil recovery (CO2-EOR) sites," *Int. J. Greenh. Gas Control*, vol. 51, pp. 369–379, Aug. 2016.

[164] G. Cooney, M. Jamieson, J. Marriott, J. Bergerson, A. Brandt, and T. J. Skone, "Updating the U.S. Life Cycle GHG Petroleum Baseline to 2014 with Projections to 2040 Using Open-Source Engineering-Based Models," *Environ. Sci. Technol.*, vol. 51, no. 2, pp. 977–987, Nov. 2017.

[165] A. Burnham, J. Han, C. E. Clark, M. Wang, J. B. Dunn, and I. Palou-Rivera, "Life-Cycle Greenhouse Gas Emissions of Shale Gas, Natural Gas, Coal, and Petroleum," *Environ. Sci. Technol.*, vol. 46, no. 2, pp. 619–627, Jan. 2012, doi: 10.1021/es201942m.